

## JGR Atmospheres

## RESEARCH ARTICLE

10.1029/2021JD034984

## Key Points:

- Per model-measurement analysis, black and brown carbon (BrC) absorption efficiencies are higher in smoke from Africa relative to the western United States
- Modeling BrC absorption with black carbon:organic aerosol (BC:OA) parameterizations improves model-observation agreement without sufficiently distinguishing regions
- A universal 1-day BrC whitening timescale in the model performs better against observations than a scheme based on OH exposure

## Supporting Information:

Supporting Information may be found in the online version of this article.

## Correspondence to:

T. S. Carter and C. L. Heald,  
[ts Carter@mit.edu](mailto:ts Carter@mit.edu);  
[heald@mit.edu](mailto:heald@mit.edu)

## Citation:

Carter, T. S., Heald, C. L., Cappa, C. D., Kroll, J. H., Campos, T. L., Coe, H., et al. (2021). Investigating carbonaceous aerosol and its absorption properties from fires in the western United States (WE-CAN) and southern Africa (ORACLES and CLARIFY). *Journal of Geophysical Research: Atmospheres*, 126, e2021JD034984. <https://doi.org/10.1029/2021JD034984>

Received 29 MAR 2021

Accepted 1 JUL 2021

## Author Contributions:

**Conceptualization:** Therese S. Carter, Colette L. Heald

**Data curation:** Therese S. Carter


















**Formal analysis:** Therese S. Carter

**Funding acquisition:** Colette L. Heald, Christopher D. Cappa, Jesse H. Kroll

**Investigation:** Therese S. Carter

**Resources:** Teresa L. Campos, Hugh Coe, Michael I. Cotterell, Nicholas W. Davies, Delphine K. Farmer, Cathryn Fox, Lauren A. Garofalo, Lu Hu, Justin M. Langridge, Ezra J. T. Levin, Shane M. Murphy, Rudra P. Pokhrel, Yingjie

## Investigating Carbonaceous Aerosol and Its Absorption Properties From Fires in the Western United States (WE-CAN) and Southern Africa (ORACLES and CLARIFY)

Therese S. Carter<sup>1</sup> , Colette L. Heald<sup>1,2</sup> , Christopher D. Cappa<sup>3</sup> , Jesse H. Kroll<sup>1,4</sup> , Teresa L. Campos<sup>5</sup> , Hugh Coe<sup>6</sup> , Michael I. Cotterell<sup>7</sup> , Nicholas W. Davies<sup>8,9</sup>, Delphine K. Farmer<sup>10</sup> , Cathryn Fox<sup>9</sup>, Lauren A. Garofalo<sup>10</sup> , Lu Hu<sup>11</sup> , Justin M. Langridge<sup>9</sup> , Ezra J. T. Levin<sup>12,13</sup> , Shane M. Murphy<sup>14</sup> , Rudra P. Pokhrel<sup>14,15</sup> , Yingjie Shen<sup>14</sup>, Kate Szpek<sup>9</sup> , Jonathan W. Taylor<sup>6</sup> , and Huihui Wu<sup>6</sup> 

<sup>1</sup>Civil and Environmental Engineering Department, Massachusetts Institute of Technology, Cambridge, MA, USA, <sup>2</sup>Earth, Atmospheric and Planetary Sciences, Massachusetts Institute of Technology, Cambridge, MA, USA, <sup>3</sup>Department of Civil and Environmental Engineering, University of California at Davis, Davis, CA, USA, <sup>4</sup>Department of Chemical Engineering, Massachusetts Institute of Technology, Cambridge, MA, USA, <sup>5</sup>Atmospheric Chemistry Division, National Center for Atmospheric Research, Boulder, CO, USA, <sup>6</sup>Department of Earth and Environmental Sciences, University of Manchester, Manchester, UK, <sup>7</sup>School of Chemistry, University of Bristol, Bristol, UK, <sup>8</sup>College of Engineering, Mathematics and Physical Sciences, University of Exeter, Exeter, UK, <sup>9</sup>Met Office, Exeter, UK, <sup>10</sup>Department of Chemistry, Colorado State University, Fort Collins, CO, USA, <sup>11</sup>Department of Chemistry and Biochemistry, University of Montana, Missoula, MT, USA, <sup>12</sup>Department of Atmospheric Science, Colorado State University, Fort Collins, CO, USA, <sup>13</sup>Handix Scientific, Boulder, CO, USA, <sup>14</sup>Department of Atmospheric Science, University of Wyoming, Laramie, WY, USA, <sup>15</sup>Now at Department of Physics, North Carolina A&T State University, Greensboro, NC, USA

**Abstract** Biomass burning (BB) produces large quantities of carbonaceous aerosol (black carbon and organic aerosol, BC and OA, respectively), which significantly degrade air quality and impact climate. BC absorbs radiation, warming the atmosphere, while OA typically scatters radiation, leading to cooling. However, some OA, termed brown carbon (BrC), also absorbs visible and near UV radiation; although, its properties are not well constrained. We explore three aircraft campaigns from important BB regions with different dominant fuel and fire types (Western Wildfire Experiment for Cloud Chemistry, Aerosol Absorption, and Nitrogen [WE-CAN] in the western United States and ObseRvations of Aerosols above CLouds and their intEractionS and Cloud-Aerosol-Radiation Interactions and Forcing for Year downwind of southern Africa) and compare them with simulations from the global chemical transport model, GEOS-Chem using GFED4s. The model generally captures the observed vertical profiles of carbonaceous BB aerosol concentrations; however, we find that BB BC emissions are underestimated in southern Africa. Our comparisons suggest that BC and/or BrC absorption is substantially higher downwind of Africa than in the western United States and, while the Saleh et al. (2014, <https://doi.org/10.1038/ngeo2220>) and FIREX parameterizations based on the BC:OA ratio improve model-observation agreement in some regions, they do not sufficiently differentiate absorption characteristics at short wavelengths. We find that photochemical whitening substantially decreases the burden and direct radiative effect of BrC (annual mean of +0.29 W m<sup>-2</sup> without whitening and +0.08 W m<sup>-2</sup> with). Our comparisons suggest that whitening is required to explain WE-CAN observations; however, the importance of whitening for African fires cannot be confirmed. Qualitative comparisons with the OMI UV aerosol index suggest our standard BrC whitening scheme may be too fast over Africa.

**Plain Language Summary** Smoke from fires has large air quality, health, and climate impacts. However, both the quantity of smoke and its ability to warm or cool the atmosphere remain poorly understood. The two major particle components of smoke (black carbon [BC] and organic aerosol [OA]) interact with incoming solar radiation in distinct ways, with BC generally absorbing light and leading to warming while OA mainly scatters radiation causing cooling. Some types of OA absorb over specific wavelengths of light; these particles are called brown carbon (BrC). Our work uses observations from the western United States and downwind of southern Africa and a global model to better understand the air quality and climate effects of fires in these regions. We find that BC emissions from fires are

Shen, Kate Szpek, Jonathan W. Taylor, Huihui Wu

**Supervision:** Colette L. Heald

**Visualization:** Therese S. Carter

**Writing – original draft:** Therese S. Carter, Colette L. Heald

**Writing – review & editing:** Therese S. Carter, Colette L. Heald, Christopher D. Cappa, Jesse H. Kroll, Teresa L. Campos, Hugh Coe, Michael I. Cotterell, Nicholas W. Davies, Delphine K. Farmer, Cathryn Fox, Lauren A. Garofalo, Lu Hu, Justin M. Langridge, Ezra J. T. Levin, Shane M. Murphy, Rudra P. Pokhrel, Yingjie Shen, Kate Szpek, Jonathan W. Taylor, Huihui Wu

**Writing – review & editing:** Therese S. Carter, Colette L. Heald, Christopher D. Cappa, Jesse H. Kroll, Teresa L. Campos, Hugh Coe, Michael I. Cotterell, Nicholas W. Davies, Delphine K. Farmer, Cathryn Fox, Lauren A. Garofalo, Lu Hu, Justin M. Langridge, Ezra J. T. Levin, Shane M. Murphy, Rudra P. Pokhrel, Yingjie Shen, Kate Szpek, Jonathan W. Taylor, Huihui Wu

underestimated in Africa. We find that the black and/or BrC observed downwind of Africa is more absorbing than those in the western United States. We show that our current model does not accurately represent the differing observed absorption strengths for BrC. Comparing the model and observations suggests that BrC loses its ability to absorb (or whitens) in the western United States, but we cannot confirm that over Africa.

## 1. Introduction

Biomass burning (BB), both wildfires and prescribed burns, emits large quantities of particulate matter (PM) globally (Akagi et al., 2011) with air quality and climate impacts across regional to global scales. Air quality degradation from smoke impairs visibility and is detrimental to human health (Johnston et al. 2012; Liu et al., 2015; O'Dell et al., 2020; Reid et al. 2016; Williamson et al., 2016) with substantial associated economic costs (e.g., Jones, 2017). Climate impacts of BB emissions include heating and cooling of Earth's atmosphere and surface caused by aerosol-radiation and aerosol-cloud interactions, as well as a decrease in planetary albedo associated with black carbon (BC) deposition on snow (Bond et al., 2013). These impacts remain uncertain and poorly constrained—in large part because the magnitudes and characteristics of different BB aerosol (BBA) species from varied fire and fuel types are not well understood.

Particulate matter from BB is dominated by carbonaceous aerosol; previous work has estimated that BB adds between  $\sim 16$  and  $34 \text{ Tg yr}^{-1}$  of aerosol to the atmosphere (Akagi et al., 2011; Bond et al., 2013; Carter et al., 2020). Globally, BB is responsible for roughly one third of all BC emissions and between 65% and 90% of organic aerosol (OA) emissions (Bond et al., 2013; Carter et al., 2020). However, uncertainties on these emissions are high; for example, estimates of BBA from the four most commonly used fire emissions inventories differ by roughly a factor of two globally with larger differences regionally (Carter et al., 2020). Important BB source regions can have both very different dominant combustion types and also fuel types—both of which are difficult to globally characterize, and thus are not adequately captured by emission inventories, particularly at high spatial and temporal resolution.

Biomass burning aerosol has three major carbonaceous constituents, which interact directly with radiation in different ways: BC, which is largely absorbing; primary OA (POA), which generally scatters but which may also absorb, and which is then referred to as brown carbon (BrC); and secondary OA (SOA), which has been shown to mostly scatter (Laskin et al., 2015). Inorganic, non-carbonaceous components are also present in BBA, but in relatively small quantities (typically  $<15\%$  of total submicron aerosol in fresh wildfire emissions) (Garofalo et al., 2019). Unlike BC, which is also emitted in low quantities (typically  $\sim 2\text{--}10\%$  of submicron mass) (Garofalo et al., 2019), these non-carbonaceous components play a minor role in radiative effects beyond direct light scattering and are not considered here. The net radiative impact of smoke is thus a complex combination of the different abundance and properties of BBA species. Previous work has reported a large spread with uncertainty in even the sign of the possible direct radiative effect (DRE or the instantaneous radiative impact) (Heald et al., 2014) of BBA from  $-0.01$  to  $+0.13 \text{ W m}^{-2}$  (Rap et al., 2013; Ward et al., 2012). The IPCC Fifth Assessment report concludes that the absorption and scattering from fires effectively offset each other, but the underlying models used do not generally have an explicit representation of BrC (IPCC, 2014).

Recent work on BBA absorption properties has provided key insights, but further work is needed to better constrain the DRE of BBA. The ability of a species to absorb light is commonly represented by the mass absorption coefficient (MAC, the absorption cross-section per unit mass with a unit of  $\text{m}^2 \text{ g}^{-1}$ ), which depends on the molecular form (Liu et al., 2020) of the absorbing species as well as aerosol shape and size. Bond and Bergstrom (2006) determined that the MAC of BC from combustion sources is  $7.5 \text{ m}^2 \text{ g}^{-1}$  at a wavelength of  $550 \text{ nm}$  for uncoated particles based on an average of  $\sim 20$  measurements. This translates to a MAC of  $6 \text{ m}^2 \text{ g}^{-1}$  at a wavelength of  $660 \text{ nm}$ , assuming an absorption Ångström exponent (AAE) of 1. Wang et al. (2014) showed that the direct radiative forcing (DRF) of BC had been previously overestimated due to an overestimate of the BC lifetime and an incorrect attribution of BrC absorption to BC. Wang et al. (2018) discussed how representing BBA as externally mixed (i.e., that the majority of OA is externally mixed with BC) is reasonable considering the low BC:OA emission ratio from BB and biofuel and typical coating thickness (Moffet & Prather, 2009; Perring et al., 2017; Schwarz, Spackman, et al., 2008). Based on several field studies

(Cappa et al., 2012; Lack et al., 2012; Moffet & Prather, 2009; Schwarz, Gao, et al., 2008; Schwarz, Spackman, et al., 2008), Wang et al. (2014) showed that applying different absorption enhancement (AE, i.e., the MAC of the internally mixed BC with coating species such as OA and inorganics, relative to the MAC of the corresponding uncoated BC) factors for the hydrophilic components of BB-emitted BC (1.5) and fossil fuel (FF)-derived BC (1.1) could help approximate the mixing state of BC and OA and thus lensing effects, and improve agreement with observations. The so-called lensing effect is when a coated BC particle with a non- or weakly absorbing shell (in fire emissions, this shell is generally composed of OA) absorbs more than the BC core alone (Bond et al., 2006; Fuller et al., 1999; Jacobson, 2000). The AE is assumed to result from coatings on BC, distinct from absorption by BrC. Other recent work that focused on combustion of fuels native to the western United States and primary particles emitted found AE factors of 1.2–1.5 for BB BC (McMeeking et al., 2014) and no larger than 1.19 (McClure et al., 2020), suggesting that the assumption of Wang et al. (2014) (used in this work) is at the high end of the estimated range. However, given that the studies cited here are mostly focused on North and central America, it is possible that the AE for smoke from Africa (where BC:OA is higher) may differ from that in the western United States. A recent study of observations downwind of Africa reported AE factors as high as 1.85 (Taylor et al., 2020).

Substantial uncertainties exist around the emission, production, and absorption properties of BrC. Biomass burning POA has been shown to be the dominant source of BrC globally. Laboratory work has shown that some SOA can also absorb (Laskin et al., 2015). Palm et al. (2020) showed, with a combination of lab and field data, that the contribution of nitroaromatics, specifically nitrocatechol, to aerosol absorption is oversized compared to its mass. However, in general, SOA has been found to be considerably less absorbing than BB POA (see for example Figure 1 in Wang et al., 2014). Some work has suggested that BrC absorption may constitute up to ~40% of total absorption of carbonaceous aerosol, but there is a large range for this value and that of BrC DRE (+0.03 to +0.6 W m<sup>-2</sup>) in the literature (Feng et al., 2013; Lin et al., 2014; Wang et al., 2014, 2018). The MAC of OA is smaller than that of BC (e.g., OA MAC at 550 nm is estimated to be 0.35 m<sup>2</sup> g<sup>-1</sup> vs. 7.5 m<sup>2</sup> g<sup>-1</sup> for uncoated BC discussed above [Bond & Bergstrom, 2006; Wang et al., 2018]). However, BrC absorption has a strong wavelength dependence with increasing absorption in the UV; studies show a range in OA MAC from 0.65 to 5.01 m<sup>2</sup> g<sup>-1</sup> at 365 nm (Jo et al., 2016; Wang et al., 2018). BrC may also undergo whitening (a decrease in absorptivity over time); limited field work to date suggests that this occurs with an e-folding time of ~1 day (Forrister et al., 2015; Wang et al., 2016).

Biomass burning aerosol emitted from fires with various fuel and combustion types has been shown to have different absorption characteristics (e.g., more flaming fires may lead to more absorbing BrC [McClure et al., 2020; Saleh et al., 2014]). However, global modeling studies have typically assumed globally uniform properties independent of combustion phase (Chung et al., 2012; Feng et al., 2013; Jo et al., 2016; Park et al., 2010; Wang et al., 2014). In addition, very little work has been done to validate model simulations of aerosol absorption, particularly from BrC (Liu et al., 2020). Challenges exist with the measurement techniques used for BBA absorption that would subsequently be used to constrain models (Liu et al., 2020). Filter-based techniques like aethalometers (Hansen et al., 1983), particle soot absorption photometers (PSAPs) (Bond et al., 1999), and continuous light absorption photometers (CLAPs) (Ogren et al., 2017) are commonly used measurement techniques but are susceptible to a variety of biases (Davies et al., 2019; Lack et al., 2008), including multiple scattering within the filter and loadings on saturated filters leading to nonlinear responses and backscatter variability due to particle size distributions (Foster et al., 2019 and references therein). An alternative approach to measuring absorption is to take the difference between extinction and scattering, as done by the cavity-attenuated phase shift PM single-scattering albedo (CAPS PM<sub>SSA</sub>) instrument. The CAPS PM<sub>SSA</sub> has high accuracy and precision but only when measured aerosol has a low single scattering albedo (Foster et al., 2019). Alternatively, photoacoustic spectroscopy (PAS), has been shown to be an unbiased and sensitive approach to measuring the absorption of dry aerosol but requires a more complex calibration (Cotterell et al., 2020, 2021; Davies et al., 2018; Foster et al., 2019 and references therein).

In the last few decades, burned area has decreased globally by 25%, but increased in some important BBA source regions like southern Africa and the western United States (Andela et al., 2017). Previous work has suggested that future trajectories in fire impacts will vary across regions (e.g., Ford et al., 2018; Val Martin et al., 2015; Yue et al., 2013). Thus, with different fire and fuel properties leading to varying smoke absorption

properties and with BB regions already experiencing a range of fire trends, it is essential that we better understand the quantity of BBA and its absorption properties globally, with at least regional granularity.

In this study, we use the GEOS-Chem chemical transport model, satellite observations, and data from three aircraft campaigns that surveyed very different fire regimes (western United States and southern Africa) to contrast the abundance and properties of carbonaceous aerosol from fires in two important BB source regions and to test the model representation of these properties.

## 2. Model and Observation Descriptions

### 2.1. The GEOS-Chem Model

We use GEOS-Chem (<https://geos-chem.org>, last access: April 24, 2019), a global chemical transport model, coupled with the rapid radiative transfer model for global circulation models (RRTMG, Iacono et al., 2008), a configuration known as GC-RT (Heald et al., 2014), to explore BBA and its absorption properties in the western United States and off the coast of southern Africa. GEOS-Chem is driven by assimilated meteorology from the Modern-Era Retrospective analysis for Research and Applications, Version 2 (MERRA-2), at the NASA Global Modeling and Assimilation Office (GMAO). We run version 12.3.0 of GEOS-Chem (<https://doi.org/10.5281/zenodo.2620535>) with a horizontal resolution of  $2^\circ \times 2.5^\circ$  and 47 vertical levels with a chemical time step of 20 min and a transport time step of 10 min as recommended by Philip et al. (2016). We perform 6-month spin-up simulations prior to the time periods of interest, July–August 2016, August–September 2017, and July–September 2018. We also perform nested simulations over North America at  $0.5^\circ \times 0.625^\circ$  (with boundary conditions from the global simulation) for comparison against WE-CAN observations (see Section 2.2) with transport and chemistry time steps of 5 and 10 min, respectively.

GEOS-Chem includes  $\text{SO}_4^{2-}/\text{NO}_3^-/\text{NH}_4^+$  thermodynamics (Fountoukis & Nenes, 2007) coupled to an  $\text{O}_3$ –VOC– $\text{NO}_x$ –oxidant chemical mechanism (Chan Miller et al., 2017; Mao et al., 2013; Travis et al., 2016) with integrated Cl–Br–I chemistry (Sherwen et al., 2016). Aerosols are modeled as fixed log-normal size distributions. Aerosol optical properties are generally from the Global Aerosol Data Set (GADS) database (Köpke et al., 1997) with updates from Drury et al. (2010) and Wang et al. (2014, 2018), which are detailed below. RRTMG calculates both longwave and shortwave atmospheric radiative fluxes. When coupled to GEOS-Chem, this calculation is performed every 3 h. Longwave and shortwave DRE at the top of the atmosphere are summed and reported as total DRE.

The standard simulation of BC in GEOS-Chem is described in Park et al. (2003). We update this simulation as described by Wang et al. (2014), including the following: the initial hydrophilic fraction for BC is set to 20% for FF/biofuel (BF) and to 70% for BB; FF BC aging is proportional to the concentration of  $\text{SO}_2$  and OH; BB/BF BC aging is specified with a 4 h e-folding time; and the BC size (log-normal distribution) for FF BC is set to a geometric mean diameter (GMD) = 60 nm and standard deviation ( $\delta$ ) = 1.6 and for BF/BB BC to GMD = 140 nm and  $\delta$  = 1.4. To account for differences in mixing state, we apply an AE from coating of BC of 1.1 for FF BC and of 1.5 for BF/BB BC. With these updates, including the AE, and using Mie Theory with input from the Global Aerosol Data Set (GADS, <http://opac.userweb.mwn.de/radaer/gads.html>) (Köpke et al., 1997), Wang et al. (2014) estimate the “best” dry MAC at 550 nm for FF BC of  $7.0 \text{ m}^2 \text{ g}^{-1}$  and for BB BC of  $9.5 \text{ m}^2 \text{ g}^{-1}$  (corresponding to uncoated MAC values of  $6.3 \text{ m}^2 \text{ g}^{-1}$  without the AE, which is substantially lower than the “best” estimate from Bond & Bergstrom, 2006 and smaller than McClure et al., 2020). The wavelength dependence of the refractive index of BB BC that we use is based on the GADS (<http://opac.userweb.mwn.de/radaer/gads.html>) (Köpke et al., 1997), a database used by many global models because it covers wavelengths from near-UV to IR. Table 1 provides more details on the MAC values for BB BC and BrC used in this work. We note that the associated AAE of BC decreases with wavelength, and is well below 1 for all visible wavelengths (referenced to 405 nm); this may underestimate the BC MAC at shorter wavelengths as discussed in Sections 3.2 and 4.

The standard primary organic aerosol (POA) simulation, used here, emits 50% of POA as hydrophobic and ages hydrophobic POA to hydrophilic POA with an atmospheric lifetime of 1.15 d (Chin et al., 2002; Cooke et al., 1999). We use OA to OC (organic carbon) ratios of 1.4 and 2.1 for hydrophobic and hydrophilic OC, respectively. The model formation of SOA follows the simple scheme described in Pai et al. (2020); SOA precursor gases from fires are emitted at 0.013 g per g CO emitted. The SOA precursor gases are then aged

**Table 1**

*BB Carbonaceous Aerosol Mass Absorption Coefficient (MAC) Values Used in the GEOS-Chem Model at Wavelengths Relevant to Comparison With Observations From the Three Aircraft Campaigns Investigated in This Study*

$\lambda$ (nm)	Intrinsic $\text{MAC}_{\text{BC}}$ ( $\text{m}^2 \text{g}^{-1}$ )	Intrinsic $\text{MAC}_{\text{BC}}$ times absorption enhancement (1.5) ( $\text{m}^2 \text{g}^{-1}$ )	Baseline $\text{MAC}_{\text{OA}}$ ( $\text{m}^2 \text{g}^{-1}$ ) for BrC	Saleh parameterization $\text{MAC}_{\text{OA}}$ ( $\text{m}^2$ $\text{g}^{-1}$ ) for BrC			FIREX parameterization $\text{MAC}_{\text{OA}}$ ( $\text{m}^2 \text{g}^{-1}$ ) for BrC		
				WE- CAN	ORACLES-2016	CLARIFY	WE- CAN	ORACLES-2016	CLARIFY
660	5.3	8.0	0.13	0.11	0.11	0.11	0.06	0.14	0.15
470	6.6	10.0	0.74	0.61	0.85	0.90	0.64	0.76	0.80
405	6.9	10.4	0.95	1.1	1.5	1.6	0.90	1.2	1.3

Abbreviations: BB, biomass burning; BrC, brown carbon; CLARIFY, Cloud-Aerosol-Radiation Interactions and Forcing for Year; ORACLES, Observations of Aerosols above Clouds and their Interactions; WE-CAN, Western Wildfire Experiment for Cloud Chemistry, Aerosol Absorption, and Nitrogen.

to SOA based on a first-order rate constant (lifetime of 1 d). We use the optical properties for “white” carbon as described in Wang et al. (2018) for SOA and FF POA. We simulate BrC by assuming that emitted BB POA is BrC, using optical properties for absorbing OA as described in Wang et al. (2018): for a dry BB POA, the MAC equals  $1.33 \text{ m}^2 \text{g}^{-1}$  at 365 nm,  $0.35 \text{ m}^2 \text{g}^{-1}$  at 550 nm, and  $0.13 \text{ m}^2 \text{g}^{-1}$  at 660 nm, which decreases with aging. The wavelength dependence of BrC is also based on Wang et al. (2018), which used the Saleh parameterization and one average BC:OA ratio globally. See Table 1 for these baseline values of  $\text{MAC}_{\text{OA}}$  at wavelengths relevant to our model-observation comparisons. We implement the whitening parametrization from Wang et al. (2018) that assumes the absorptivity of OA decreases at a rate related to the concentration of OH (with a rate constant corresponding to a 1-day whitening e-folding time when assuming  $[\text{OH}]$  equal to  $5 \times 10^5 \text{ molec cm}^{-3}$ ) and that absorptivity does not drop below 25% of the starting value. Alternative parameterizations for the properties of BrC are considered in Section 4.

Anthropogenic emissions (including fossil and biofuel sources) of both BC and POA follow the CEDS global inventory (Hoesly et al., 2018) with regional inventories used instead when available, including NEI2011v1 over the United States (US EPA, 2015) scaled to 2013 (scale factors were not available beyond 2013), APEI over Canada, and DICE-Africa over Africa (Marais & Wiedinmyer, 2016). Trash burning emissions are from Wiedinmyer et al. (2014). Aircraft emissions are from the AEIC inventory (Simone et al., 2013; Stettler et al., 2011). Biogenic emissions are calculated online from the MEGANv2.1 emissions framework (Guenther et al., 2012). Fire emissions, emitted into the boundary layer, are from the GFED4s inventory (Giglio et al., 2018; van der Werf et al., 2017), specified on a daily timescale. GFED4s was selected because previous work has shown that it generally matches observations well and is typically in the middle of the range of emission estimates across inventories (Carter et al., 2020). Global total emissions of BC are 9.0 Tg and of OC are 32.5 Tg in 2018 in our simulations, but it is important to note that emissions vary year to year.

## 2.2. In Situ Observations

The Western Wildfire Experiment for Cloud Chemistry, Aerosol Absorption, and Nitrogen (WE-CAN) summer campaign used the NSF/NCAR C-130 aircraft to survey wildfires (mostly forest fires) in the western United States from July 24 to September 13, 2018 (see Figure 1 for flight tracks). Several of the large fires in California and Oregon in the summer of 2018 are visible in the smoke emissions shown in Figure 1, including the Mendocino Complex, Carr, and Ferguson Fires. WE-CAN targeted smoke in the near-field (<6 h since emission) by sampling close to the fire and systematically sampling downwind to intercept the same parcel of air multiple times to track evolution of smoke over time. BC mass concentrations were measured using a single-particle soot photometer (SP2; DMT; Schwarz, Gao, et al., 2008). For WE-CAN, the SP2 detection range for BC mass equivalent diameters is  $\sim 90\text{--}500 \text{ nm}$ , and the calibration uncertainty is estimated to be 30%. BC mass outside the SP2 detection range was not estimated for the WE-CAN data set. However, based on observations of BC size distributions from biomass burning (Schwarz, Gao, et al., 2008), it is expected that the SP2 measurements captured the majority of the BC mass; this is similarly true for the ORACLES and CLARIFY campaigns. When sampling in plumes, the SP2 sample line was diluted with HEPA-filtered, ambient air to prevent signal saturation. OA mass concentrations were measured using a

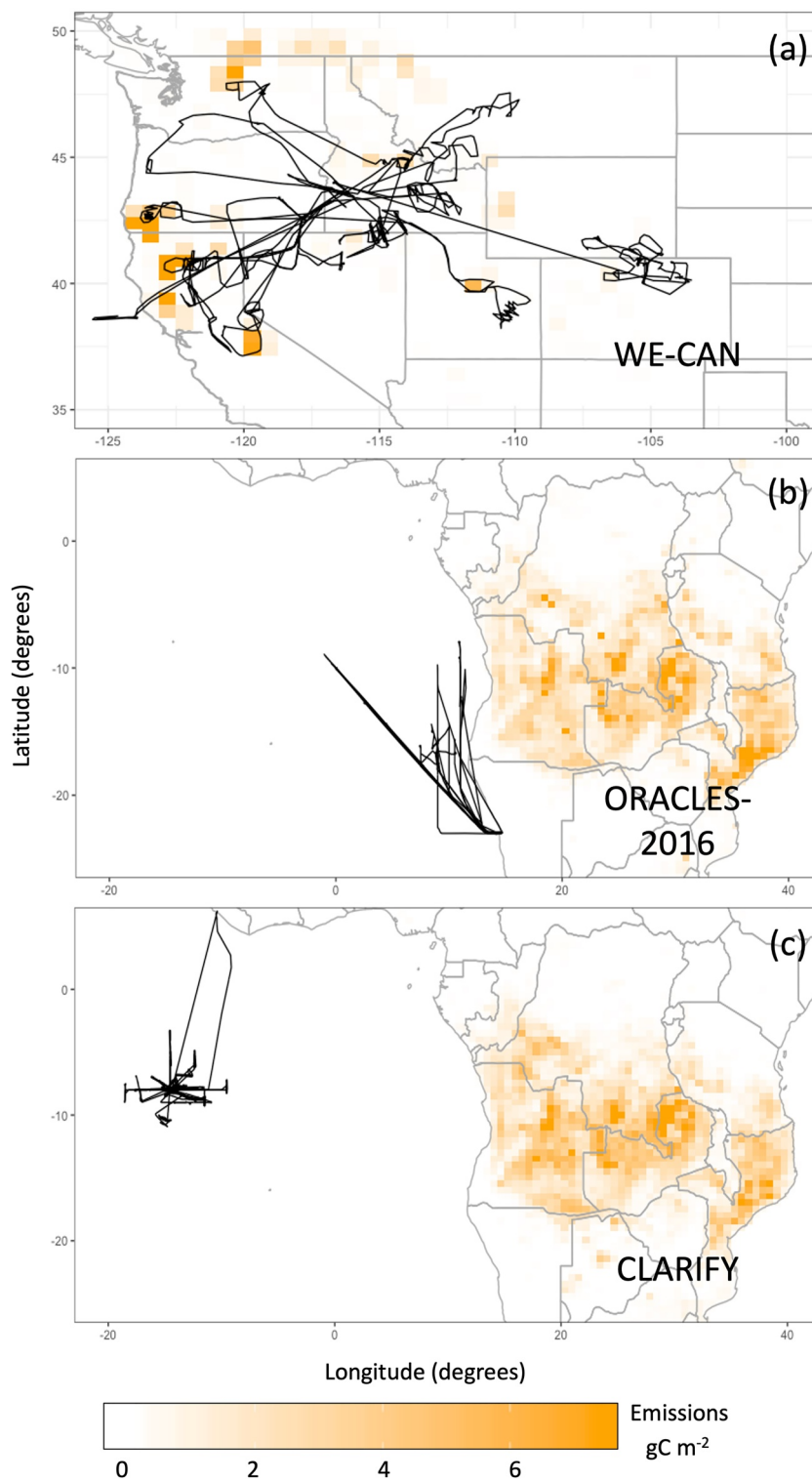


**Figure 1.** Flight tracks of the (a) Western Wildfire Experiment for Cloud Chemistry, Aerosol Absorption, and Nitrogen (WE-CAN), (b) Observations of Aerosols above Clouds and their interactions (ORACLES-2016), and (c) Cloud-Aerosol-Radiation Interactions and Forcing for Year (CLARIFY) campaigns overlaid on total biomass burning aerosol emissions from GFED4s during the months of each respective campaign (July–September 2018 for WE-CAN, August–September 2016 for ORACLES-2016, and August 2017 for CLARIFY). Note that the underlying maps are not on the same scale.

high-resolution time-of-flight aerosol mass spectrometer (HR-AMS; Aerodyne Inc.) with a detection range for vacuum aerodynamic particle diameter of 70–~1,000 nm and an estimated uncertainty of 35% (Garofalo et al., 2019). Carbon monoxide (CO) was measured using two instruments: a quantum cascade laser instrument (QCL; CS-108 miniQCL, Aerodyne, Inc.) and a gas analyzer utilizing cavity ring-down spectroscopy (G2401-m WS-CRD; Picarro). Garofalo et al. (2019) noted that the QCL instrument had a better measurement precision for CO concentrations than that of the Picarro gas analyzer. Therefore, we use the concentration measurements from the QCL instrument in our analyses here. Acetonitrile, a useful BB tracer, was measured using a proton transfer reaction time of flight mass spectrometer with an uncertainty in mixing ratios of 15% (PTR-ToF-MS 4000; Ionicon Analytik; [Müller et al., 2014; Permar et al., 2021]). A photoacoustic absorption spectrometer (PAS) was used to measure total absorption with two dry (RH < 15%) channels at 405 and 660 nm (Foster et al., 2019).

ORACLES (ObseRvations of Aerosols above CLouds and their intEractionS) was a 5-year investigation with three intensive observation periods in roughly August–September of 2016, 2017, and 2018 that surveyed off the Atlantic coast of southern Africa. This campaign was designed to study key processes that regulate the climate impacts of African BBA—a large global source of particles, responsible for ~1/3 of all global BBA emissions, but one that is severely understudied. The smoke sampled during this campaign was primarily aged outflow from savanna fires and some agricultural fires (~2–15 days after emission [Pistone et al., 2019]). In this work, we focus on the 2016 deployment out of Walvis Bay, Namibia; although, we also compare simulations with 2017 data with very similar results (not shown)—consistent with small interannual variability in southern African fires. The BBA measured during the 2018 deployment were of a lower concentration compared to other years of the ORACLES campaign, likely because most of the 2018 sampling was in October as opposed to the more dominant fire months of August and September (Ichoku, 2020; Zuidema et al., 2018). We use data from 13 flights performed by the NASA P-3 aircraft in 2016. Figure 1 shows that emissions are geographically more extensive in the southern African region than the region sampled in WE-CAN but that peak emission rates in the ORACLES region are lower. We note here that we have saturated the WE-CAN plot in Figure 1 to the same scale as that for ORACLES, but the maximum fire emissions are ~2 times larger for the WE-CAN campaign. BC mass concentrations were measured using an SP2 with a particle size detection range of 70–700 nm and an uncertainty of 25%. A Time of Flight Aerosol Mass Spectrometer (ToF-AMS) was used to measure OA mass concentrations for particles with diameters within the detection range of 30–1,000 nm and an uncertainty of 30%. An ABB/Los Gatos Research CO/CO<sub>2</sub>/H<sub>2</sub>O analyzer was used for CO concentration measurements with an uncertainty of 1%. Two Radiance Research PSAPs were used to measure dried aerosol total absorption at 470, 530, and 660 nm. Instrument noise levels were 0.5 Mm<sup>-1</sup> for a 240–300 s sample; additional details are given in Pistone et al. (2019). During this campaign, the multiple scattering from this filter-based measurement potentially led to a high bias in the PSAP signal (Pistone et al., 2019). To partially address this, we use the average wavelength-corrected PSAP observations provided by Pistone et al. (2019), which have been shown to be less biased than the wavelength-specific values whose use resulted in an unphysical increase in the absorption Ångström exponent (Pistone et al., 2019; Zuidema et al., 2018); this does not alter the conclusions presented here.

The Cloud-Aerosol-Radiation Interactions and Forcing for Year 2017 (CLARIFY) campaign aimed to improve model estimates of the direct, semi-direct, and indirect radiative forcings of BBA. Full details of the campaign are given in Haywood et al. (2021). We use data from 13 flights from the deployment of the FAAM Bae-146 aircraft out of Ascension Island for 4 weeks during August 2017. This deployment sampled the same broad source region as ORACLES-2016 but further west; thus the air had been transported and therefore aged further (~4–8 days from emission (Taylor et al., 2020)). BC mass concentrations were measured using an SP2 with a particle size detection range of 102–533 nm, an uncertainty of 17% (Taylor et al., 2020), and a 100% detection efficiency for particles with 1–143 fg BC per particle. A compact Time of Flight Aerosol Mass Spectrometer (cToF-AMS) was used to measure OA mass concentrations with a detection range for particle vacuum aerodynamic diameter of 50–700 nm (Taylor et al., 2020) and an uncertainty of 30%. An Aero-Laser AL5002 was used to measure CO concentrations with an uncertainty of ±2.8 ppb at 1 Hz. Measurements of dry (RH < 10%) aerosol absorption at 405, 514, and 660 nm were made using photoacoustic spectroscopy using the EXSCALABAR PAS instrumentation described by Davies et al. (2018, 2019) and Cotterell et al. (2020, 2021) with an uncertainty on the absorption instrument of 8% (Davies et al., 2019).

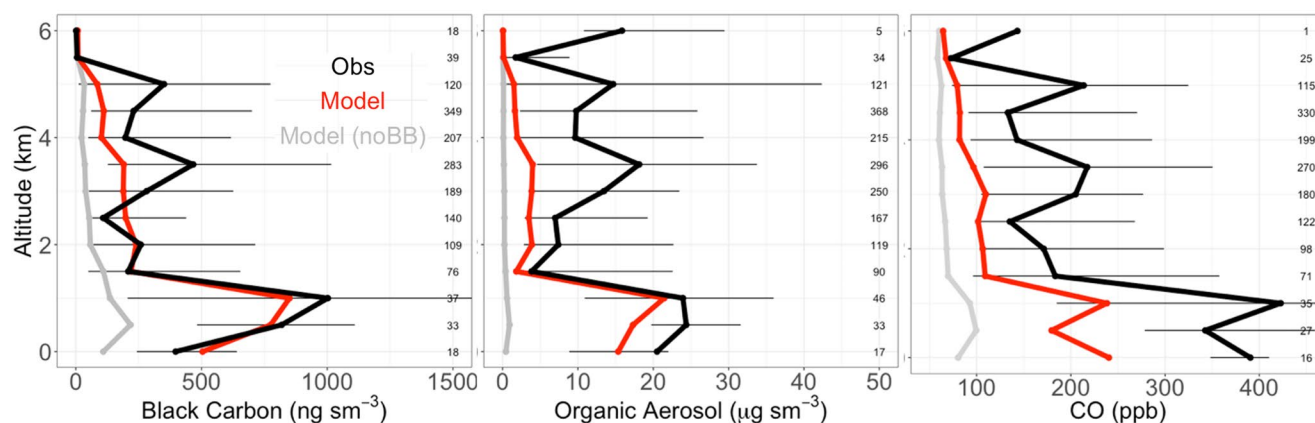


**Figure 2.** The median vertical profiles of black carbon, organic aerosol, and CO concentrations (shown in 0.5 km bins) from the Western Wildfire Experiment for Cloud Chemistry, Aerosol Absorption, and Nitrogen campaign. Observations (black) are compared with model simulations (red) and a simulation with no fire emissions (noBB) in gray. Horizontal bars show the 25th–75th percentile range of measurements in each vertical bin. The number of observations in each bin is given on the right side of each panel. Aerosol concentration measurements and simulations are reported at standard conditions of temperature and pressure (STP: 273K, 1 atm).

All aerosol mass concentrations across campaigns are shown at standard temperature and pressure: STP (273K, 1 atm). For comparison with airborne measurements, the model was sampled to the nearest grid box both temporally and spatially to each flight track using 1 min aircraft data. We then average both the model and the observations to the model grid box.

In addition to the WE-CAN flight observations in the contiguous US (CONUS), we also use IMPROVE (Interagency Monitoring of Protected Visual Environments, <http://vista.cira.colostate.edu/improve/>, last access: February 24, 2020) surface observations from 155 sites in 2018 and compare against 24 h averaged model results to further constrain anthropogenic BC in CONUS. BC is measured using a PM<sub>2.5</sub> size-selective filter-based thermal method in this network (Chow et al., 2007).

### 3. Campaign Comparisons

We use observations from the WE-CAN, ORACLES-2016, and CLARIFY campaigns to test how well our model captures mass concentrations and absorption properties of BBA from different fire source regions. In Sections 3.1 and 3.2, we compare observations with our baseline simulation.

#### 3.1. Mass Concentration Comparisons

##### 3.1.1. WE-CAN

We first compare median vertical profiles of BC, OA, and CO concentrations observed during WE-CAN with model-simulated concentrations (Figure 2). We find that the model is biased substantially low for OA and CO across most altitudes but matches observed BC quite well from roughly 3 km to the surface with some underestimate at higher altitudes. Below 3 km, simulated OA is biased low by 30% and CO by 41% while BC is only biased low by 7%. We note that SOA contributes ~5% of the simulated OA at all altitudes, in good agreement with observed percentages (Palm et al., 2020). Because this is a strongly plume-targeted campaign, BB is the dominant emission source for all three species, as indicated by a noBB simulation in gray, which shows much lower concentrations. Thus, given that fires are the dominant source for all three, one might expect similar model performance for all three species.

The low bias of OA and CO is consistent with a campaign that targeted many fresh fire plumes, given that Eulerian models generally have trouble reproducing sub grid features (Eastham & Jacob, 2017; Rastigejev et al., 2010). The comparisons of Figure 2 suggest that the higher resolution nested grid used here is not sufficient to capture near-field plumes sampled during WE-CAN. Figure S1 shows that concentrations of acetonitrile (a useful BB tracer) during WE-CAN are considerably higher (254 ppt median) than during two



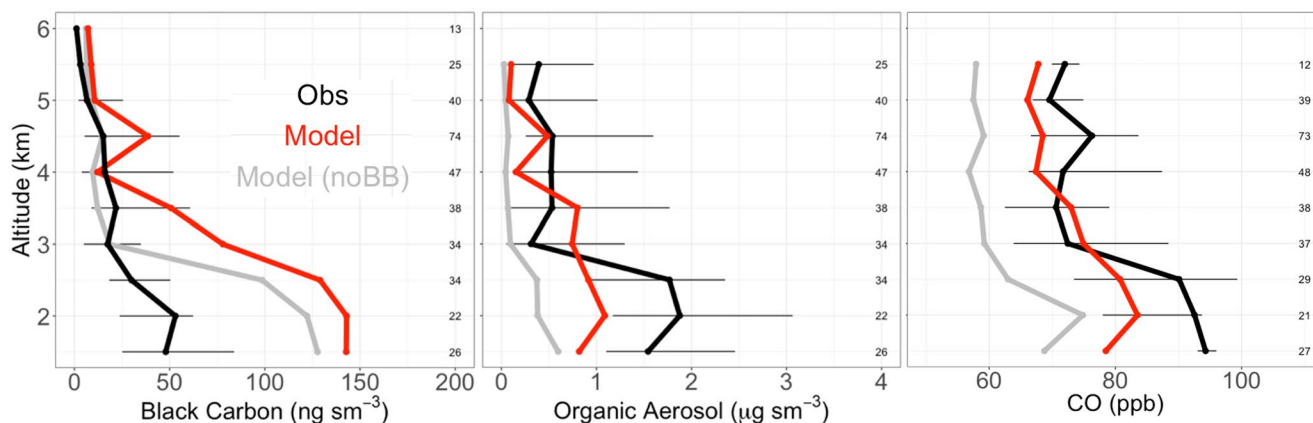


**Figure 3.** The median vertical profiles of black carbon, organic aerosol, and CO concentrations with the same conventions as Figure 2 with results filtered to include only data coincident with the bottom 25th percentile of observed acetonitrile. We note that the y axis starts at 1.5 km because the lowest quartile of acetonitrile is found above this altitude.

other well-characterized, fire-influenced campaigns: DC3 (167 ppt, May–June 2012 in the southeastern and south-central United States) and the boreal portion of ARCTAS (213 ppt, June–July 2008 in boreal Canada). Furthermore, the WE-CAN measurements show a pronounced tail extending to very high acetonitrile concentrations that are not present in the observations for the DC3 and ARCTAS campaigns. For reference, previous work has suggested that 225 ppt is a potential cutoff for fire influence (Aruffo et al., 2016), indicating that more than half of the observations during WE-CAN are within concentrated smoke plumes that are challenging for the model to resolve. This plume-targeted sampling strategy likely accounts for the low model bias for OA and CO.

While the model is biased low with respect to observations of both OA and CO, as previously noted, model-simulated BC better captures observations in this fire-influenced regime. Figure 3 shows the same comparisons for BC, OA, and CO when filtered to include only the lowest 25th percentile (<159 ppt) acetonitrile to isolate the observations with the least fire influence (or more aged/diluted fire influence). We note that concentrations filtered for the lowest 25th percentile of acetonitrile are considerably lower (roughly an order of magnitude) than the medians for the full data set shown in Figure 2. We see from the noBB (gray lines) simulations, that even for the lowest acetonitrile concentrations, much of the OA and CO is due to fires, whereas the BC is largely due to other sources (fossil fuels). We show that the model is better able to capture the least fire-influenced OA and CO between 3 and 5.5 km (compared to Figure 2), though an underestimate persists in the lowest 2 km given the predominance of fire OA and CO even at these lower acetonitrile levels. However, the model clearly overestimates the least fire-influenced BC, indicating that anthropogenic BC emissions from the 2011 NEI may be overestimated in this region.

To investigate the suggestion from Figure 3 that the anthropogenic BC emissions are overestimated, we compare simulated surface BC concentrations with observations from the IMPROVE network. To focus on anthropogenic emissions, we compare modeled and observed mean wintertime (December 2017 to February 2018) BC concentrations in CONUS when fire emissions should be negligible, with a few notable exceptions outside of the “WE-CAN region” including the Thomas fire in Southern California. In the wintertime, biofuel BC from home heating/fireplaces may be more important in certain regions; based on the inventories used here, and, in this example, BF BC contributes ~13% of all US BC emissions at this time of year. Figure S2 shows that, spatially, the model is in reasonable agreement with the IMPROVE observations, but with a large positive bias (34% normalized mean bias (NMB) for CONUS and 90% for the specific geographic region where WE-CAN sampled). Taken together, our analysis indicates that anthropogenic BC emissions are too high in the 2011 NEI. This is consistent with previous work that also used NEI 2011 for anthropogenic BC emissions (e.g., Carter et al., 2020; Kim et al., 2015; Wang et al., 2018); although, our work suggests that the overestimate is even higher than in these previous studies, perhaps because we use 2013 emissions here (see Section 2.1). Annual anthropogenic BC emissions in the recently released (full release in April 2020) 2016 NEI inventory are ~40% lower than in the 2011 NEI, suggesting that updated inventories

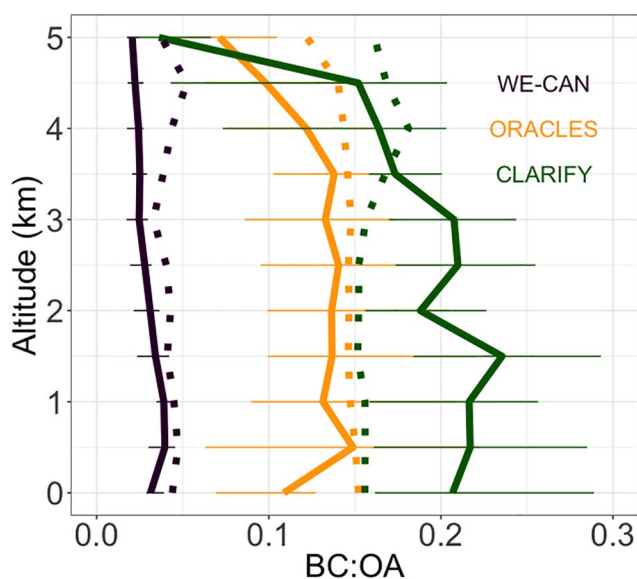


**Figure 4.** The median vertical profiles of the black carbon:organic aerosol (BC:OA) ratio (shown in 0.5 km bins) from Western Wildfire Experiment for Cloud Chemistry, Aerosol Absorption, and Nitrogen (WE-CAN) (in purple), Observations of Aerosols above Clouds and their interactions (ORACLES-2016) (in orange), and Cloud-Aerosol-Radiation Interactions and Forcing for Year (CLARIFY) (in green) with both ORACLES-2016 and CLARIFY using scaled up BB BC emissions. Observations (solid lines) are compared with model simulations (dotted lines). The WE-CAN comparisons have been filtered to remove the data corresponding to the lowest 25th percentile of acetonitrile (see Section 3.1.1). Horizontal bars show the 25th–75th percentile range of measurements averaged in each vertical bin.

may be more consistent with our analysis. A more detailed spatial and temporal exploration of anthropogenic BC emissions across the United States is needed.

In an effort to minimize the impact of any fossil fuel emissions bias on our analysis of BBA, we remove the data associated with the bottom 25th percentile acetonitrile in the analysis that follows. The filtered modeled BC vertical profiles (not shown) demonstrate the same low bias as shown in Figure 2 for OA and CO. Using this filtered data, we find that the observed median vertical profile of the BC:OA ratio is well captured by the model with only a slight overestimate, likely due to the residual influence of overestimated fossil fuel emissions (Figure 4). Thus, when focusing on fire-influenced points, the model captures well the observed BC:OA ratio while underestimating the magnitude of observed mass concentrations of both.

### 3.1.2. ORACLES-2016 and CLARIFY

The ORACLES-2016 and CLARIFY campaigns sampled downwind (by generally 2 or more days) of fires in southern Africa. CLARIFY is substantially downwind from ORACLES-2016 (i.e., the plume is likely to have descended further and become more aged). Stratocumulus sheets also tend to be more broken in the CLARIFY region around Ascension Island. This sampling of aged smoke provides a better opportunity for the model to reproduce observations, in contrast to WE-CAN's sampling of sub-model grid plumes. Figure 5 shows a comparison of vertical profiles of simulated and observed concentrations of BC, OA, and CO during the 2016 ORACLES and 2017 CLARIFY campaigns. The noBB simulation (shown in gray) demonstrates that BC, OA, and CO concentrations are all dominated by smoke in these campaigns.

Figure 5 shows that the model generally captures the magnitude of observed OA and CO mass concentrations during ORACLES-2016 and CLARIFY, with the exception of a substantial low bias aloft from ~3 to 5 km. This underestimate likely results from the representation of clouds in the MERRA-2 assimilated meteorology used in GEOS-Chem. A multi-model study investigating ORACLES-2016 found that cloud cover was significant during many flights and that both GEOS-5 and GEOS-Chem underestimate the top of smoke plumes (Shinozuka et al., 2020). Haywood et al. (2021) also showed significant cloud cover during the CLARIFY campaign. Das et al. (2017) show that GEOS-Chem (using MERRA meteorology) aerosol transport off the coast of southern Africa is characterized by a sharp descent in aerosol plumes from ~4 to 5 km due to excessive subsidence over the ocean in the MERRA product, producing an aerosol layer which is located closer to the surface than observed with CALIOP. This vertical displacement is similar to the low bias shown in our simulation of ORACLES-2016 and CLARIFY (Figure 5). This low bias is somewhat larger for CLARIFY, potentially because the CLARIFY observations are further from the source and are thus affected by longer subsidence timescales. Given our use of assimilated meteorology, it is not possible to explore how BC and OA might respond to differences in entrainment and other cloud related processes. However, we do find that the model bias is highest under high humidity conditions, supporting a cloud-related mechanism for this biased vertical profile. We tested the impact of recent wet deposition updates related to cloud liquid water and scavenging efficiencies for GEOS-Chem (Luo et al., 2019), which minimally impacted our comparison. An injection height sensitivity test based on Fischer et al., (2014), which emits a percentage of emissions into the free troposphere, yielded little change in the simulated vertical profile. Thus, the bias aloft is likely associated with cloud representation in MERRA-2 and not injection height issues. Self-lofting of the absorbing aerosol may also contribute to the discrepancies above boundary layer (Haywood et al., 2021), and more work is needed to explore this mechanism.

Figure 5 shows a model underestimate of observed BC mass concentrations by a factor of ~2.3 during ORACLES-2016, which can be attributed to fire emissions given the negligible anthropogenic influence on BC

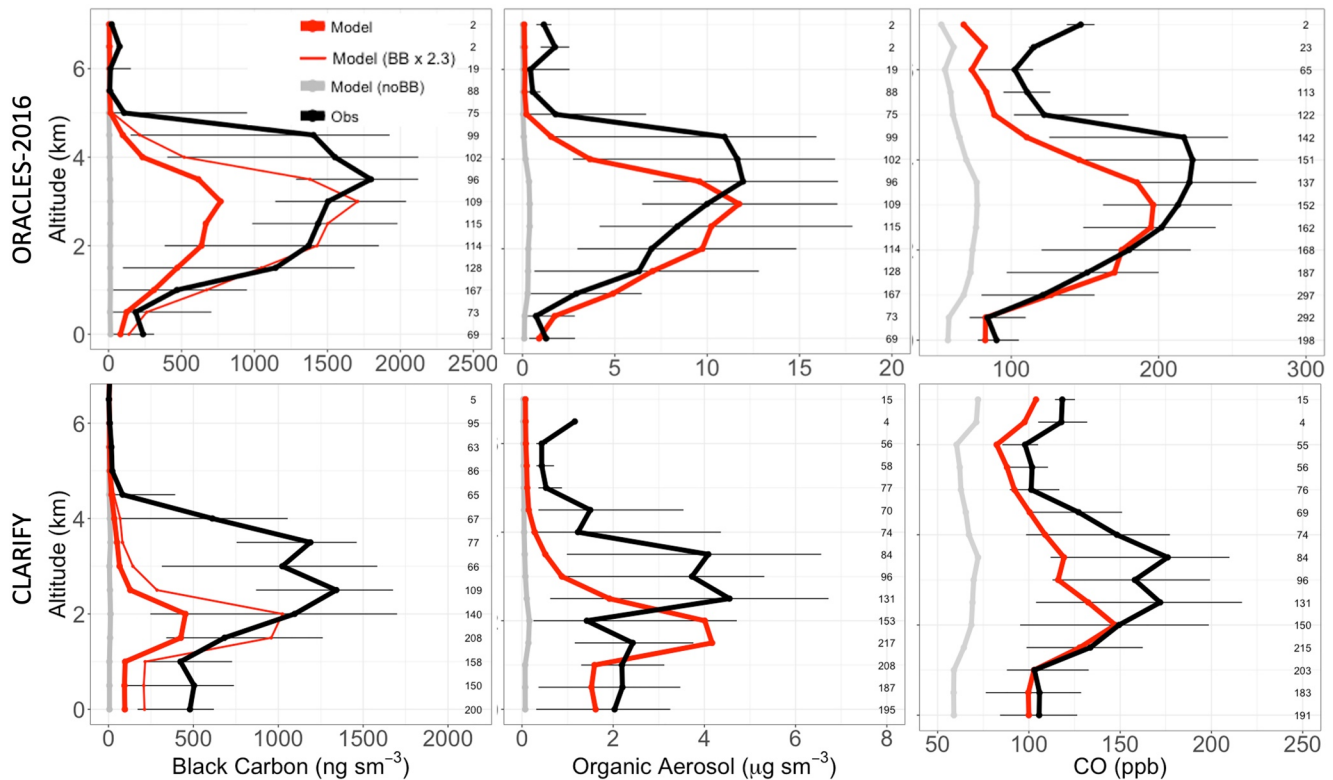


**Figure 5.** The median vertical profiles of black carbon, organic aerosol, and CO mass concentrations (shown in 0.5 km bins) from the Observations of Aerosols above CLouds and their intEractionS-2016 (top) and Cloud-Aerosol-Radiation Interactions and Forcing for Year (bottom) campaigns. Observations (black) are compared with model simulations (red; thinner red line shows simulation with biomass burning black carbon emissions scaled up by a factor of 2.3) and a simulation with no fire emissions (noBB) in gray. Horizontal bars show the 25th–75th percentile range of measurements averaged in each vertical bin. The number of observations in each bin is given on the right side of each panel. Aerosol concentration measurements and simulated values are reported at standard conditions of temperature and pressure (STP: 273K, 1 atm).

(gray lines). A study exploring the DACCIWA campaign in western Africa provides additional evidence for underestimated BB BC emissions in this region; they scale fire emissions (in this case from the GFAS inventory, which, for this region and season, are within 25% of the GFED4s inventory) by 3.4 in GEOS-Chem to match observations (Haslett et al., 2019). Ramo et al. (2021) suggest that burned area in sub-Saharan Africa is underestimated by 63% (compared to GFED4s in 2016) due to missing contributions from small fires, which can be better detected with higher resolution satellite products. In addition, a recently updated emission factor (EF) compilation (Andreae, 2019) confirms that a higher BC EF is reasonable for the vegetation type fires (savanna) dominating the ORACLES-2016 and CLARIFY campaigns. The inventory that we use (GFED4s) uses 0.37 g/kg dry matter (DM) burned for savanna BC emissions while the updated Andreae (2019) paper suggests a value of 0.53 g/kg DM with a standard deviation across studies of 0.35 g/kg DM. Scaling up the BC savanna EF by a factor of  $\sim 2.3$  falls within the range presented in Andreae (2019). Scaling up BB BC emissions by this factor does not entirely remedy the CLARIFY model-observation bias (Figure 5), potentially because different fires were sampled than during ORACLES-2016. Observations of additional chemical tracers for anthropogenic and biomass burning activity are needed to understand these source differences from Africa, as well as additional observations over the source region.

In the following analyses for ORACLES-2016 and CLARIFY, we scale up BB BC emissions in southern Africa by a factor of 2.3. While this scaling factor is somewhat arbitrary, it is supported by 3 years of comparison against ORACLES data and additional literature evidence detailed above. It is not sufficient to explain the CLARIFY underestimate, but a more sophisticated inverse model would be needed to correct emissions to match both ORACLES and CLARIFY. This is beyond the scope of this work. While we do not scale savanna EFs elsewhere as we do not have the observations to test such scaling, it is possible that savanna BB BC EFs are similarly underestimated in other regions, and more work is needed to investigate this. The BC:OA ratio

is particularly well captured during ORACLES-2016 (Figure 4) when including these scaled up BB emissions, so we focus on the ORACLES-2016 data set in our discussions of the smoke absorption properties downwind of Africa in addition to including a comparison with CLARIFY.

For ORACLES, we show comparisons here only for data collected during the 2016 deployment, but given the limited interannual variability in fires in the region, the observed magnitudes and the model comparisons are consistent for 2017 and 2018 albeit with small differences discussed in Section 2.2.

### 3.2. Absorption Comparisons

Comparisons of vertical profiles of simulated and observed total absorption (not shown) demonstrate model underestimates consistent with the aforementioned low model bias of mass concentrations (Figures 2 and 7). We, therefore, focus on the mass-normalized absorption (i.e., the MAC) under dry conditions, as the MAC is an intrinsic aerosol optical property independent of mass loadings and associated biases. This minimizes the effect of mass underestimates associated with WE-CAN plume sampling, vertical transport biases off of Africa, and BC emissions biases affecting CLARIFY.

Because the total absorption measurements do not distinguish between BC and OA contributions to absorption, our strategy is to first look at the  $MAC_{BC}$  (i.e., the absorption coefficient divided by the BC mass concentration) at 660 nm where BC absorption should dominate. We then explore the MAC of total BBA or  $MAC_{BC+OA}$  (i.e., the absorption coefficient divided by the summed mass concentrations for BC and OA) at shorter wavelengths (where both BC and BrC contribute substantially to absorption). This enables us to investigate the role of BrC absorption informed by our knowledge of BC absorption. Modeled and observed MAC quantities are calculated in the same way to enable comparison. Note that critical to this analysis of the  $MAC_{BC+OA}$  is the model's ability to capture the BC:OA observed in these two very different regions of the world, as shown in Figure 4. These ratios are predicted well by our model for WE-CAN and ORACLES, but are not captured as well for the CLARIFY measurement region, rendering the CLARIFY comparisons somewhat less useful for constraining the model optical properties. We further note that uncertainty in the average BC:OA ratio increases with altitude with fewer observations and lower concentrations. Here we focus on absorption constraints at two wavelengths only (limited by the observations from WE-CAN), however additional measurements that can better constrain the wavelength dependence of absorption may provide further insight.

MAC calculations are only performed when the observed and modeled BC mass concentrations (or the combined BC and OA mass concentration, if calculating  $MAC_{BC+OA}$ ) are greater than  $0.6 \mu\text{g sm}^{-3}$  and for which the corresponding extinction values, if available from the datasets, are greater than  $10 \text{ Mm}^{-1}$  (as suggested by Shinozuka et al., 2019 to reduce noise as instruments approach their detection limit). Our results are robust to this filtering; filtering reduces the range of estimated MAC but not central values.

#### 3.2.1. WE-CAN

At 660 nm, total aerosol absorption is generally dominated by BC, owing to the low absorptivity of BrC relative to BC at this wavelength (McClure et al., 2020; Pokhrel et al., 2017). Figure 6 shows good agreement between the observed (black) and modeled (red)  $MAC_{BC}$  at 660 nm. The median values for observed and simulated  $MAC_{BC}$  at 660 nm ( $11.29$  and  $12.03 \text{ m}^2 \text{ g}^{-1}$ , respectively) are higher than values for BB-dominated BC absorption alone (see Section 2.1 for assumptions regarding BB BC absorptivity). While the absorption from OA is much lower at longer wavelengths (see Section 2.1), there is so much OA in the smoke sampled during WE-CAN (Figure 2) that its contribution to total absorption at 660 nm is considerable, and its inclusion in the model reconciles the predicted  $MAC_{BC}$  with observed values (Figure 6). Our simulations of  $MAC_{BC}$  at 660 nm use an AE of 1.5 for BB BC (as in Wang et al., 2014, see Section 1 for details). However, our model assumption for the intrinsic BB  $MAC_{BC}$  at 660 nm ( $5.3 \text{ m}^2 \text{ g}^{-1}$ , without accounting for the AE) is lower than other values in the literature (e.g.,  $6.25 \text{ m}^2 \text{ g}^{-1}$ ; [Bond & Bergstrom, 2006]). As noted in Section 1, the AE assumed in our model for BB BC is at the high end of literature estimates from North America, increasing the plausibility that it is partially accounting for a lower intrinsic BB  $MAC_{BC}$ .

At 405 nm, the role of BrC absorption is more important than at longer wavelengths. We calculate the  $MAC_{BC+OA}$  at this shorter wavelength. These values are inherently much smaller than  $MAC_{BC}$  given the

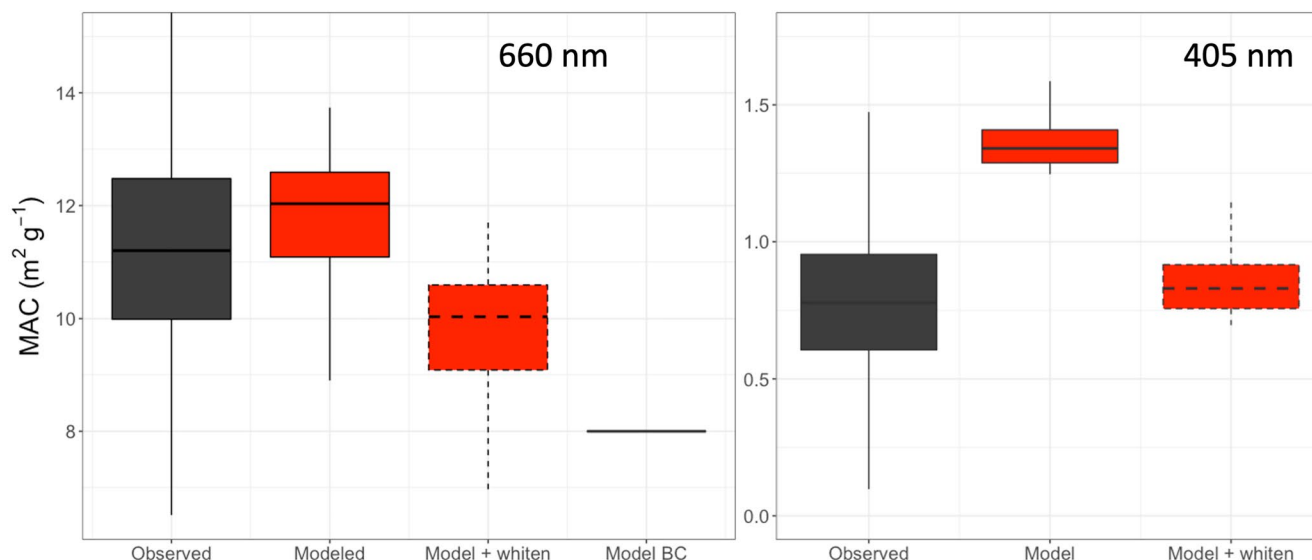


**Figure 6.** Boxplot summaries of the mass absorption coefficient (MAC) observed (black) and modeled with GEOS-Chem (red) for the Western Wildfire Experiment for Cloud Chemistry, Aerosol Absorption, and Nitrogen campaign. Values at 660 nm are shown on the left ( $MAC_{BC}$  = total absorption divided by black carbon [BC] mass concentration) and at 405 nm on the right ( $MAC_{BC+OA}$  = total absorption divided by the summed BC and organic aerosol mass concentration). Model BC refers to the  $MAC_{BC}$  when only accounting for absorption from BC in the model. The horizontal bar is the median. The box shows the 25th to the 75th percentile, and the whiskers show 1.5 times the interquartile range. The inclusion of BrC whitening is denoted with dashed lines.

preponderance of OA, but overall absolute absorption is higher at 405 nm than at 660 nm. We show in Figure 6 that modeled  $MAC_{BC+OA}$  (median value of  $1.34 \text{ m}^2 \text{ g}^{-1}$ ) is biased high at 405 nm and is toward the upper range of observations (median of  $0.78 \text{ m}^2 \text{ g}^{-1}$ ). As shown in Figure 4, the model generally captures the average BC:OA ratio during WE-CAN. Correcting the small high bias due to the residual influence of overestimated fossil fuel emissions reduces the simulated  $MAC_{BC+OA}$  by only  $\sim 15\%$ . It is also highly unlikely that this difference at 405 nm is the result of overestimates in the absorptivity of BC, given that  $MAC_{BC}$  is well captured by the model at longer wavelengths and that, if anything, the GADS BC AAE (0.53 from 405 to 655 nm) is low. Modeled BrC absorption at this wavelength is substantial (more than 1/2 of total absorption); therefore, photochemical whitening of these particles may play an important role in determining the  $MAC_{BC+OA}$ . Alternatively, the prescribed BrC absorption may be overestimated. However, we note that the good agreement at 660 nm makes this less likely. To investigate the impact of whitening at 405 nm, we use the parameterization from Wang et al. (2018) based on OH exposure. While WE-CAN is characterized by relatively near-field sampling, air masses in the region contain both fresh plumes and aged emissions from the surrounding fires. As a result, whitening of BrC decreases the simulated  $MAC_{BC+OA}$  considerably, bringing our modeled  $MAC_{BC+OA}$  (median of  $0.83 \text{ m}^2 \text{ g}^{-1}$ ) into good agreement with observed  $MAC_{BC+OA}$ . This corresponds to a  $MAC_{OA}$  of  $\sim 0.4 \text{ m}^2 \text{ g}^{-1}$  at 405 nm, or about 40% of the assumed  $MAC_{OA}$  for primary BB. The whitening scheme has an effect on the  $MAC_{BC}$  at 660 nm (median drops by  $\sim 2 \text{ m}^2 \text{ g}^{-1}$ ), and remains in agreement with the bottom of the interquartile range of observations. This suggests that, in the western United States, whitening should be considered when modeling BrC absorption and that the parameterization of Wang et al. (2018) does a reasonable job in capturing the magnitude of this effect.

### 3.2.2. ORACLES-2016 and CLARIFY

As in comparisons with WE-CAN observations, we focus on MAC during ORACLES-2016 and CLARIFY because the vertical absorption profiles show the same vertical bias seen in the mass concentrations. Figure 7 shows that the 660 nm  $MAC_{BC}$  observed during ORACLES-2016 (median value of  $9.30 \text{ m}^2 \text{ g}^{-1}$ ) are lower than those during WE-CAN (median  $11.29 \text{ m}^2 \text{ g}^{-1}$ ). In our framework, this is expected based on the differing BC:OA ratios for these two campaigns (see Figure 4) and thus a smaller contribution to absorption from OA downwind of Africa. The LASIC campaign in 2016 partially overlapped with ORACLES-2016 and found higher  $MAC_{BC}$  at 660 nm ( $10.7 \text{ m}^2 \text{ g}^{-1}$ ); the surface site was located on Ascension Island (Zuidema et al., 2018) and thus was further from the fire source and likely sampled more aged aerosol. During

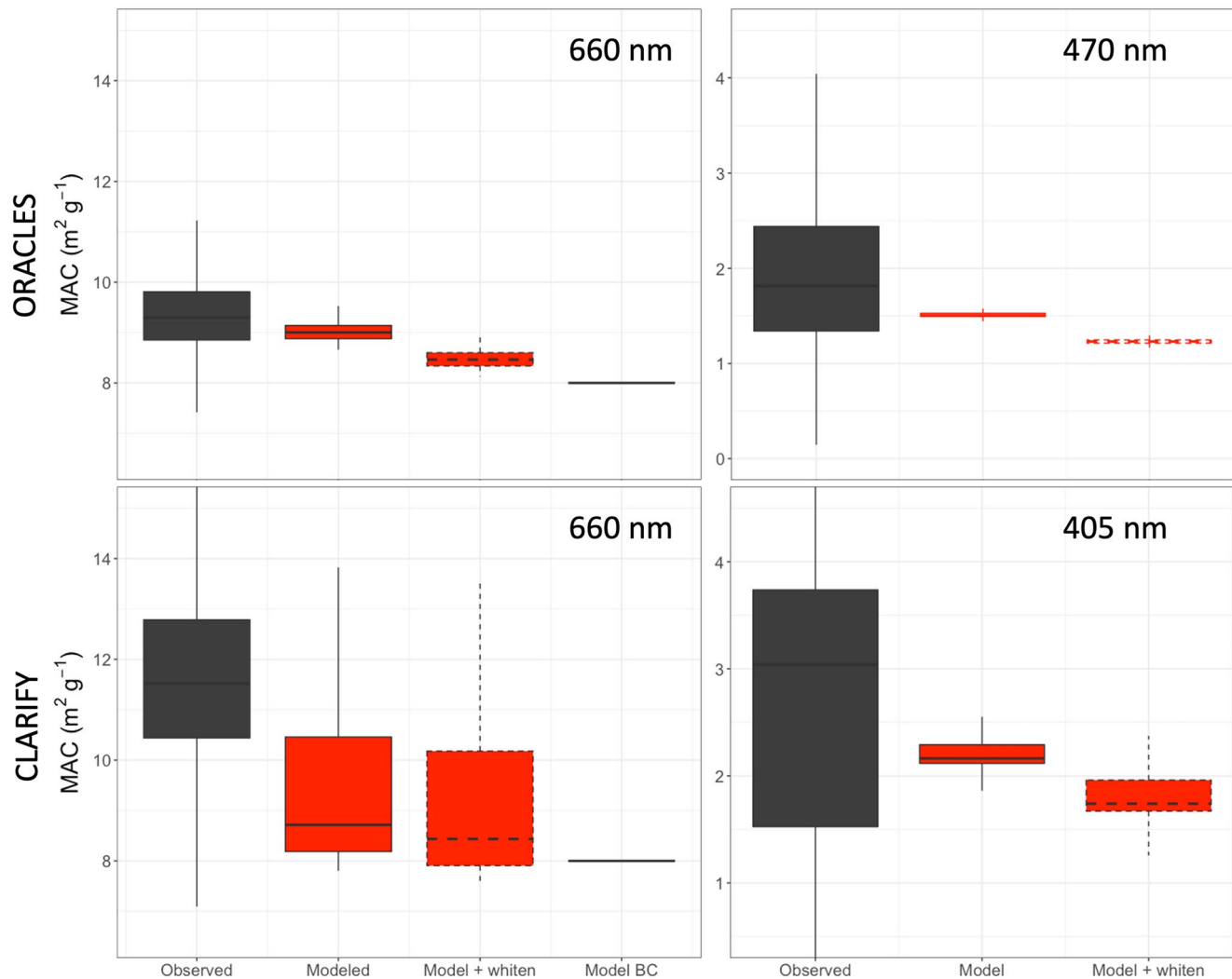


**Figure 7.** Boxplot summary of observed and simulated ObseRvations of Aerosols above CLouds and their intERactionS-2016 and Cloud-Aerosol-Radiation Interactions and Forcing for Year MAC<sub>BC</sub> at 660 nm on the left and MAC<sub>BC + OA</sub> at 470 and 405 nm, respectively, on the right. The conventions of this boxplot are described in Figure 6.

CLARIFY, the median observed MAC<sub>BC</sub> at 660 nm is considerably higher ( $11.52 \text{ m}^2 \text{g}^{-1}$ ) than during ORACLES-2016. CLARIFY sampled more aged BBA and previous studies report that these BBA exhibit some of the highest levels of coating thicknesses observed in field measurements (and thus have a higher AE due to the lensing effect) as it was transported further from the continental source region (see Figure 1 for the campaign flight tracks) (Taylor et al., 2020). While the uncertainties around sampled aerosol lifetime are large, Taylor et al. (2020) suggest that CLARIFY aerosol was sampled 4–8 days from emissions, potentially larger than some of the estimates from Pistone et al. (2019) and references therein for ORACLES-2016 (2–15 days with potentially an emphasis on 2–5 days). The two campaigns also employ different instrumentation: CLARIFY employed highly sensitive and accurate in-situ measurements (PAS) while ORACLES-2016 employed filter-based measurements (PSAP), which has higher systematic biases, with overestimates of absorption observed up to 45%. The differences in observed MAC<sub>BC</sub> are within measurement uncertainty; although, it is noteworthy that the ORACLES-2016 MAC<sub>BC</sub> is lower than the CLARIFY MAC<sub>BC</sub>, despite the potential for a positive bias in the ORACLES-2016 observations. Other possible explanations for the difference in observed MAC<sub>BC</sub> at 660 nm include an underlying MAC<sub>OA</sub> that differs between the two campaigns. However, given the high BC:OA downwind of Africa (Figure 4), OA is not likely to make such a large contribution to total absorption at these wavelengths.

Figure 7 shows that the model underestimates the  $MAC_{BC}$  at 660 nm downwind of southern Africa. Model values are similar for ORACLES-2016 and CLARIFY (8.91 and 8.72  $m^2 g^{-1}$ , respectively), as our current model scheme uses a fixed AE of 1.5 globally, which may not be a good representation of real world conditions downwind of Africa (Ko et al., 2020). Given higher BC:OA ratios for ORACLES and CLARIFY compared to WE-CAN, OA contributes less to the simulated  $MAC_{BC}$  at 660 nm. However, the contribution ( $\sim 0.9 m^2 g^{-1}$  for ORACLES,  $\sim 0.7 m^2 g^{-1}$  for CLARIFY) is not negligible. Taylor et al. (2020) suggest that a BC AE of 1.85 (applied to an intrinsic  $MAC_{BC}$  from Bond and Bergstrom (2006), that is higher than we use here) is required to correctly predict the observed  $MAC_{BC}$  during CLARIFY—this AE includes the contribution of OA absorption at 660 nm. Keeping our OA absorption properties fixed, we estimate that we would need to increase our BC AE to 2 (or that the AE applied to an intrinsic  $MAC_{BC}$  from Bond & Bergstrom, 2006 would need to be 1.8, similar to the values from Taylor et al., 2020) to match the observed  $MAC_{BC}$  at 660 nm in CLARIFY. A smaller increase in AE to 1.6 is needed to reconcile the model with observations during ORACLES at 660 nm. This may suggest that the BC in the somewhat fresher ORACLES-2016 outflow was less thickly coated compared to CLARIFY.

At shorter wavelengths, the observed  $MAC_{BC+OA}$  is higher during CLARIFY (median 3.04  $m^2 g^{-1}$ ) than for ORACLES-2016 (median 1.81  $m^2 g^{-1}$ ), due largely to the difference in the measurement wavelength (470 nm for ORACLES-2016 and 405 nm for CLARIFY). Given the higher BC:OA ratio downwind of Africa (Figure 4), BC makes a much larger contribution to absorption at shorter wavelengths than seen for WE-CAN. This increases the  $MAC_{BC+OA}$  and also suggests that the difference in  $MAC_{BC}$  seen at 660 nm between ORACLES-2016 and CLARIFY also contributes to the difference in  $MAC_{BC+OA}$  seen in Figure 7. For ORACLES in 2017 and 2018, the comparisons between observed and modeled MAC are similar to Figure 7, with 2018 showing somewhat higher observed  $MAC_{BC+OA}$  at shorter wavelengths (not shown).

At these shorter wavelengths, our baseline simulated  $MAC_{BC+OA}$  (median value of 1.51  $m^2 g^{-1}$  for ORACLES-2016 at 470 nm and 2.10  $m^2 g^{-1}$  for CLARIFY at 405 nm) also underestimates the observed  $MAC_{BC+OA}$  by 16% and 31%, respectively; though, the former is within measurement uncertainties. The larger model bias for CLARIFY compared to ORACLES-2016 can be partly reconciled by considering the model underestimate of the BC:OA for CLARIFY (Figure 4). Scaling up BC concentrations to correct this bias for CLARIFY increases the model value to  $\sim 2.37 m^2 g^{-1}$  (equivalent to a 22% underestimate). The model bias in  $MAC_{BC}$  at 660 nm likely contributes to the bias at shorter wavelengths as well. If we apply the BC AE of 1.6 and 2 for ORACLES-2016 and CLARIFY, respectively, estimated from the 660 nm comparisons to the shorter wavelengths, we reduce the model bias at the shorter wavelengths to 10% and 11% for ORACLES-2016 and CLARIFY, respectively. These differences lie within measurement uncertainties. If the model BC AAE (from GADS) is underestimated, the contribution of BC at short wavelengths may in fact be considerably larger. Including BrC whitening exacerbates the discrepancy at all wavelengths. Though, whitening decreases the  $MAC_{BC+OA}$  less downwind of Africa than during WE-CAN, consistent with a larger BC:OA downwind of Africa. We conclude that either (a) a higher AAE for BC (and thus more absorbing BC at short wavelengths) or (b) more absorbing BrC (with whitening) or (c) no photochemical whitening of BrC is required downwind of Africa to fully reconcile the model and observations. It is possible that some combination of these factors may explain the observations. In addition, Figure 7 shows that observed  $MAC_{BC}$  and  $MAC_{BC+OA}$  are much more variable than our simulated MACs. This suggests that using one number for OA MAC and for the AE does not capture the variability in absorption properties. The model also underestimates the variability in the observed BC:OA (particularly for CLARIFY).

The observations demonstrate that BBA from African fires is roughly a factor of 3 more absorbing than from fires in the western United States at short wavelengths (at 405 nm,  $MAC_{BC+OA}$  of 3.04  $m^2 g^{-1}$  for CLARIFY, compared to 0.78  $m^2 g^{-1}$  for WE-CAN). This is due, in large part, to higher BC loadings downwind of Africa relative to OA. This effect is captured by the model, which simulates the higher BC:OA observed downwind of Africa relative to the western United States (Figure 4). However, after accounting for the differing BC content, the model absorptivity remains biased low downwind of Africa. Our comparisons at longer wavelengths suggest that increasing the AE of BC (as in Taylor et al., 2020) reduces this gap. We attribute the remaining underestimate of the  $MAC_{BC+OA}$  to more absorbing BC (achieved with a higher BC AAE) and/or more absorbing BrC (or little photochemical whitening). We note that mixing state and the resulting absorption enhancement are a complex function of particle size, coating thickness, and morphology. Our

model scheme here does not dynamically simulate these factors, but rather applies a fixed AE to BC. While we acknowledge that this is a limitation of such a global model scheme, these mixing state considerations would need to translate to a wavelength dependent effect on absorption to explain the model-observation discrepancies at short wavelengths discussed here. More work is needed to better understand the role of mixing state of smoke and its impact on absorption. However, previous studies have shown that BrC absorption increases with BC:OA ratio (McClure et al., 2020; Saleh et al., 2014), consistent with our contrast of Africa and the western United States, and we therefore consider this as a possible explanation for our results in what follows.

#### 4. Impact of Alternate BrC Absorption Parameterizations

The stronger absorption at shorter wavelengths observed in smoke from African fires compared to western US fires (that cannot be attributed to higher BC content of smoke alone), in addition to the high variation in observed absorption properties from different sources or even years, imply that BrC absorption from fires should not be treated as constant. Saleh et al. (2014) found that absorption of BrC increases as a function of BC:OA ratio in laboratory measurements. McClure et al. (2020), using data from the FIREX 2016 Lab experiment in Missoula, MT, extended the Saleh work and developed their own parameterization for BrC absorption as a function of BC:OA. Figure 4 shows that the ORACLES-2016 and CLARIFY campaigns exhibited significantly higher BC:OA ratios than WE-CAN (by a factor of  $\sim 4$ – $7$ ), consistent with generally more flaming fires in southern Africa. The model generally captures the difference between the two campaign regions. These varying BC:OA ratios suggest that a parameterization keyed to this factor has the potential to better describe the difference in BrC absorption in the western United States and the southern African outflow as observed in Section 3. We note that our baseline BrC absorption properties from Wang et al. (2018) are calculated by using one globally averaged BC:OA ratio within the Saleh et al. parameterization; in this section when we refer to the Saleh parameterization, we are referring to the full parameterization which varies as a function of BC:OA. The Saleh et al. (2014) and McClure et al. (2020) parameterizations are described in detail in the SI, the latter is referred to as the “FIREX” parameterization in what follows. We explore here whether these parameterizations can better capture the observations during WE-CAN, ORACLES-2016, and CLARIFY.

While the BC:OA ratio is much lower in the western United States than downwind of Africa, when the Saleh et al. parameterization is applied to WE-CAN and ORACLES-2016, the resulting BrC imaginary refractive index  $k$  (responsible for absorption) at short wavelengths (405 and 470 nm) is similar (and generally higher) for both regions. This is the result of offsetting changes to both the  $k$  at 550 nm and the AAE used to calculate the absorption at shorter wavelengths (see SI for further details).

The FIREX parameterization produces  $MAC_{OA}$  values more than twice as high downwind of Africa compared to during WE-CAN at 660 nm, and  $\sim 50\%$  higher at 405 nm. Thus, while the Saleh et al. parameterization does go beyond assuming fixed absorption properties for BrC, it does not fully achieve our goal of representing the different brownness observed for fires in the western United States and downwind of Africa. The FIREX parameterization produces a larger difference between campaigns at longer wavelengths because the  $MAC_{OA}$  (and  $k$ ) is more sensitive to the BC:OA ratio than in the Saleh parameterization at these wavelengths, particularly in the observed and simulated WE-CAN BC:OA range (0.03–0.05).

We implement the Saleh et al. (2014) and the FIREX schemes for BrC absorption in GEOS-Chem for comparison against the three campaigns (Figure 8). We use the modeled BC:POA ratio in these parameterizations given that SOA here contributes  $<5\%$  of simulated OA mass. Given that the model generally captures the overall BC:OA ratio, we do not expect this simplification to affect our results. At 660 nm, using the Saleh parameterization does not change the  $MAC_{BC}$  significantly from the baseline simulation. At these same wavelengths the FIREX parameterization agrees well with the WE-CAN observations at 660 nm, improves agreement with the CLARIFY observations relative to both the baseline and Saleh, and overestimates observations during ORACLES-2016. The increase in BrC absorption at long wavelengths downwind of Africa with the FIREX parameterization removes much (all) of the earlier underestimate of  $MAC_{BC}$  for CLARIFY (ORACLES) seen in Figure 7, suggesting that an underestimate of BrC absorption could explain these results.



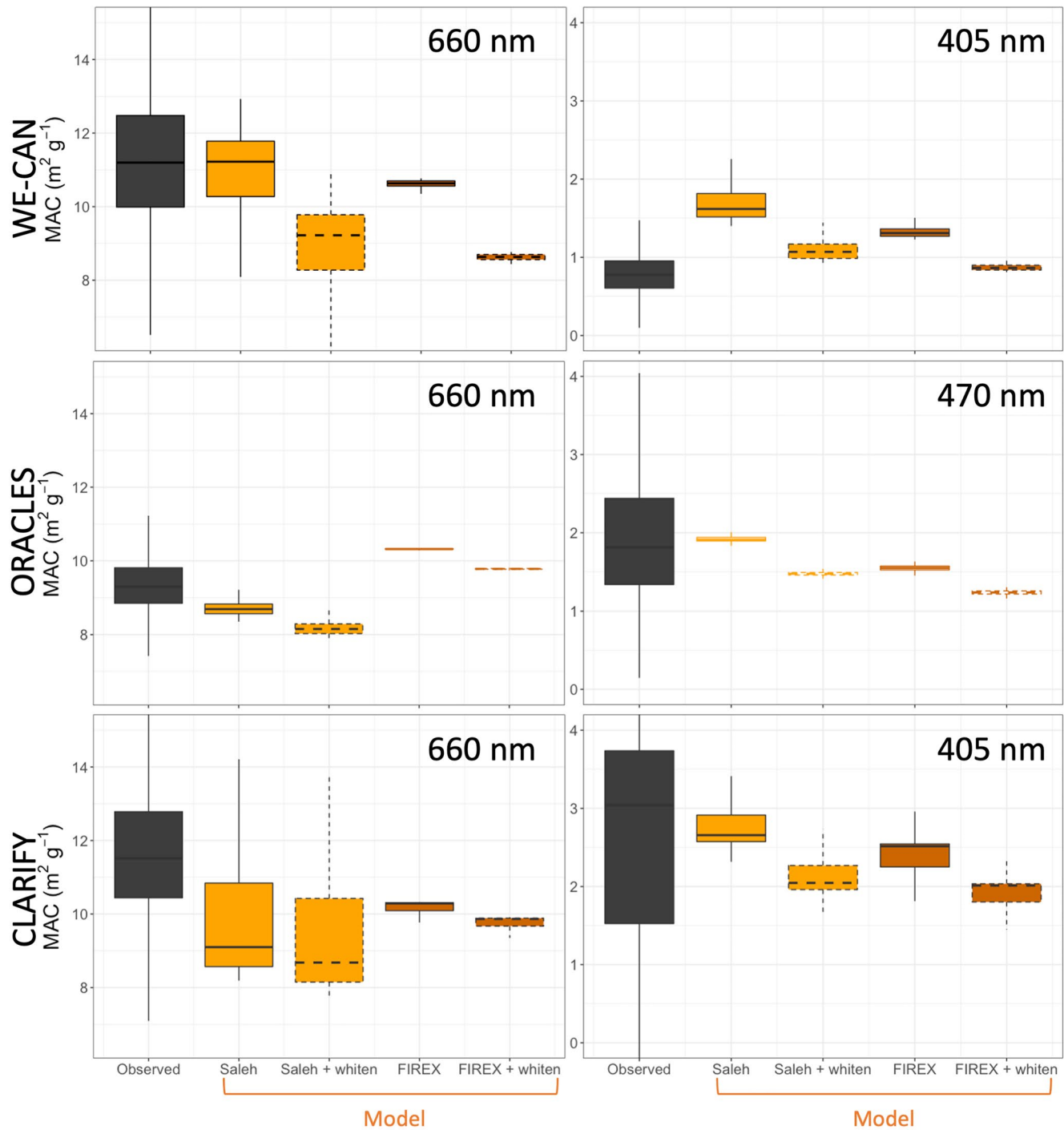


**Figure 8.** Boxplot summary of observed (black) and simulated  $MAC_{BC}$  at 660 nm on the left and  $MAC_{BC + OA}$  on the right at 405 nm for Western Wildfire Experiment for Cloud Chemistry, Aerosol Absorption, and Nitrogen (top) and Cloud-Aerosol-Radiation Interactions and Forcing for Year (bottom) and at 470 nm for ObseRvations of Aerosols above CLouds and their intERactionS-2016 (middle). Simulations using the Saleh et al. (2014) parameterization are shown in yellow and those using the FIREX parameterization in light brown. The conventions of this boxplot are described in Figure 6.

Figure 8 shows that at shorter wavelengths, using BrC parameterizations based on BC:OA ratios leads to overall increases in modeled  $MAC_{BC + OA}$  relative to the baseline (labeled “Model”) simulations—with the Saleh parameterization producing slightly larger values than the FIREX parameterization. Both parameterizations overestimate  $MAC_{BC + OA}$  during WE-CAN and improve model agreement with observations

downwind of Africa (compared to our baseline simulation). At these short wavelengths, the FIREX parameterization produces a less biased simulation for WE-CAN, but the Saleh parameterization is a better match for observations downwind of Africa. Adding photochemical whitening reduces the  $MAC_{BC + OA}$ , bringing simulated values closer to observations for WE-CAN, but degrading the comparisons downwind of Africa. In particular, photochemical whitening in combination with the FIREX parameterization results in simulated values below the lower bounds of the interquartile range of ORACLES-2016 observations. However, correcting a likely model underestimate in the BC AAE (and thus increasing the intrinsic MAC of BC) could bring us back into agreement with observations at short wavelengths. These comparisons support the need for photochemical whitening during WE-CAN (or a considerable lower intrinsic MAC for BrC than assumed with any of the FIREX, Saleh, or baseline parameterizations), but make it challenging to draw conclusions as to whether the observations support the use of a whitening parameterization for African fires.

Taylor et al. (2020) suggest that less than 11% of the absorption at 405 nm during CLARIFY was attributed to BrC, using measured MAC at 405 and 514 nm and the AAE of BC from 514 to 655 nm to estimate the absorption fraction due to BrC and an assumption of no BrC absorption at 655 nm. With the Saleh and FIREX parameterizations we attribute 48% and 35%, respectively, of absorption at 405 nm to BrC (when including whitening) during CLARIFY—these estimates are more than triple the contribution estimated by Taylor et al. (2020) for this highly aged aerosol plume, but are similar to other literature estimates of BrC absorption percentages of up to ~40% (Wang et al., 2018 and references therein). Given a likely model underestimate in the AAE of BC, our model values are likely an upper limit.

Our analysis indicates that observed brownness in the two BB regions could be different and that a parameterization that accounts for the observed elevated BrC absorptivity of African fires relative to western US fires may be necessary to capture observations during ORACLES-2016 and CLARIFY. However, using either the Saleh et al. or FIREX parameterizations does not fully account for this difference. Though, the FIREX parameterization better distinguishes smoke properties from fires in the western United States and versus Africa at longer wavelengths. At shorter wavelengths, a parameterization that results in lower BrC absorption at low BC:OA (WE-CAN) and higher BrC absorption at higher BC:OA (ORACLES-2016/CLARIFY) would better match these observations. It is possible that we are not representing another potential explanation for the different absorption of BrC in the two regions: recent work has shown that under conditions with very high primary BC:OA ratios from biomass combustion (such as savanna burning in Africa), a first stage of BrC enhancement happens after emission, owing to formation of highly absorbing SOA, and before whitening (the whitening may result from less-absorbing SOA formation in those experiments) (Cappa et al., 2020; Wu et al., 2021).

These results are further complicated by several factors. First, the fire emissions inventory does not allow BC and OA emissions to vary with either burn conditions nor sub-fuel types in the fire emissions inventory used here; GFED4s does not capture rapidly evolving burn conditions (fire temperature, intensity, etc.) and aggregates major fuel categories, such as savannas, grasslands, and shrubs together. Thus, the simulated BC:POA represents the result of average burn conditions. Variability, or indeed bias, in the representation (or airborne sampling) of these fuel types and burn conditions could drive an inaccurate implementation of the two BC:OA parameterizations. Second, our implementation of the two BC:OA parameterizations in GEOS-Chem also, by necessity, uses total BC:POA rather than the concentrations of carbonaceous aerosols from fires alone (tagging the BC:POA for fires only is an additional computational expense). Because modeled anthropogenic BC is biased slightly high during WE-CAN, using the overall, rather than BB-only, BC concentrations to parameterize BrC absorption is an imperfect representation of this lab-based parameterization. Third, the GEOS-Chem optical properties (MAC) are based on Mie theory which use refractive indices as well as particle size. If there is a mismatch between the particle size in the observations versus the model, this could lead to additional differences and to MAC values that differ between the baseline results and calculations using the FIREX parameterization, especially for Africa. Indeed, Mie theory pertains to homogeneous spheres, while BBA aerosols are known to adopt a wide variety of internal mixing states and particle morphologies (Kahnert & Kanngießer, 2020). These discrepancies with the underlying assumptions for Mie theory are a further potential source of model bias. Finally, the differences in absorption instrumentation used across the three campaigns also complicate our ability to draw broad conclusions from our model-observations comparisons. However, the PAS instruments, used during both WE-CAN and CLARIFY,

are known to be more sensitive, much faster (less averaging over long time-scales required for a useable measurement), and less biased than filter-based methods, such as the PSAP used during ORACLES-2016, especially under the dry conditions in these studies. There has been limited observational validation of smoke optical properties used in 3D models as explored here. The challenges outlined above imply that there remain opportunities to bridge laboratory parameterizations, field observations, and models.

## 5. Photochemical Whitening and the Radiative Impact of BrC

We use OMI near-UV aerosol index (AI) observations as a qualitative constraint on the spatial distribution of BrC and the potential role of photochemical whitening. Outflow from central Africa provides an ideal case study as it is dominated by smoke (e.g., Denjean et al., 2020; Hammer et al., 2018) (Figure 9), unlike the western United States where absorption from fires is confounded by anthropogenic sources. There is also minimal dust in the southern African outflow region at this time of year, enabling a focus on BrC in this region (e.g., Hammer et al., 2016). The UVAI is a qualitative parameter for detecting the presence of absorbing and scattering aerosol in the atmosphere and is sensitive to BrC and relatively insensitive to BC (e.g., Hammer et al., 2016). We use the Level-3 Aura/OMI Near UV Global Aerosol Data Products OMAERUVd product of UVAI at 1° resolution and regrid to the GEOS-Chem grid of 2° × 2.5° to enable comparison. Larger UVAI values indicate more absorption. UVAI values are higher off the coast of southern Africa relative to the western United States generally and during each campaign's deployment year (not shown), consistent with the in situ measurements that suggest BrC produced by flaming fires (e.g., those that dominate African burning [Wu et al., 2020]) is more absorbing than that from less-flaming fires (like the forest fires of the western United States) and with previous work (e.g., Hammer et al., 2016, 2018).

Figure 9 shows the region off the coast of southern Africa where the smoke plume is well-defined. The OMI UVAI product shows an abrupt change at the coastline. Two factors may contribute to this, namely that (a) this region is quite cloudy, which complicates retrievals, and (b) the retrievals are more reliable over land (Hammer et al., 2018; OMI Team, 2012), potentially explaining the observed change. While the values over the ocean may be less reliable, their relative magnitude still provides a good qualitative perspective on the decay of BrC absorption over time. BrC concentrations (as well as the UVAI) decrease due to dilution in the outflow, possible SOA formation that increases the ratio of scattering aerosol in the outflow, and whitening of BrC. An increasing inorganic fraction over time may also contribute to increasing scattering. Implementing whitening significantly decreases the total column BrC concentrations relative to a simulation without whitening. Low UVAI values are observed as far west as Ascension Island, especially as compared to the area close to the African coast where a large plume is visible and where ORACLES-2016 generally sampled.

Figure 9d compares the BrC column-integrated concentrations from simulations with no whitening, with the standard whitening, and with a slower whitening with the OMI UVAI observations plotted against longitude. The standard whitening scheme is based on two studies in different regions (Forrister et al., 2015 in the western United States and Wang et al., 2016 in the Amazon), which both suggested a 1-day photochemical lifetime, indicating that there is not strong regional variance. As described in Section 2.1, the GEOS-Chem parameterization of this process is dependent on OH levels, and equivalent to the observed 1 day at global mean average OH levels. However, given the higher [OH] in the southern African region (mean of  $\sim 3 \times 10^6$  molec cm<sup>-3</sup>), whitening timescales are much faster there ( $\sim 4$  h using the standard whitening scheme instead of 1 day). We thus run a sensitivity study that fixes the whitening timescale to 1 day globally. Peak simulated column concentrations of BrC in African outflow are roughly a factor of eight larger when neglecting whitening versus using our standard whitening parameterization, or a factor of 1.15 larger when comparing a simulation without whitening with a simulation using a slower whitening time scale. BrC emissions accumulate as you move westward over the continent (roughly 12° to 40°) in all three simulations, with the whitening process quickly counteracting some of this increase in BrC concentrations (Figure 9d). Thus, with whitening, much less BrC is exported from the continent and a more rapid decline in BrC concentrations is also observed in the outflow. The rate of decrease of the OMI UVAI observations off the coast is best matched by the simulation without whitening; although, the slower whitening simulation shows reasonable agreement as well. This suggests that the whitening time scale for smoke downwind of Africa is likely 1 day (consistent with previous field studies) or longer, and that [OH] may not be a good proxy for whitening timescales in all regions. It is also possible that the slower whitening timescale is, at

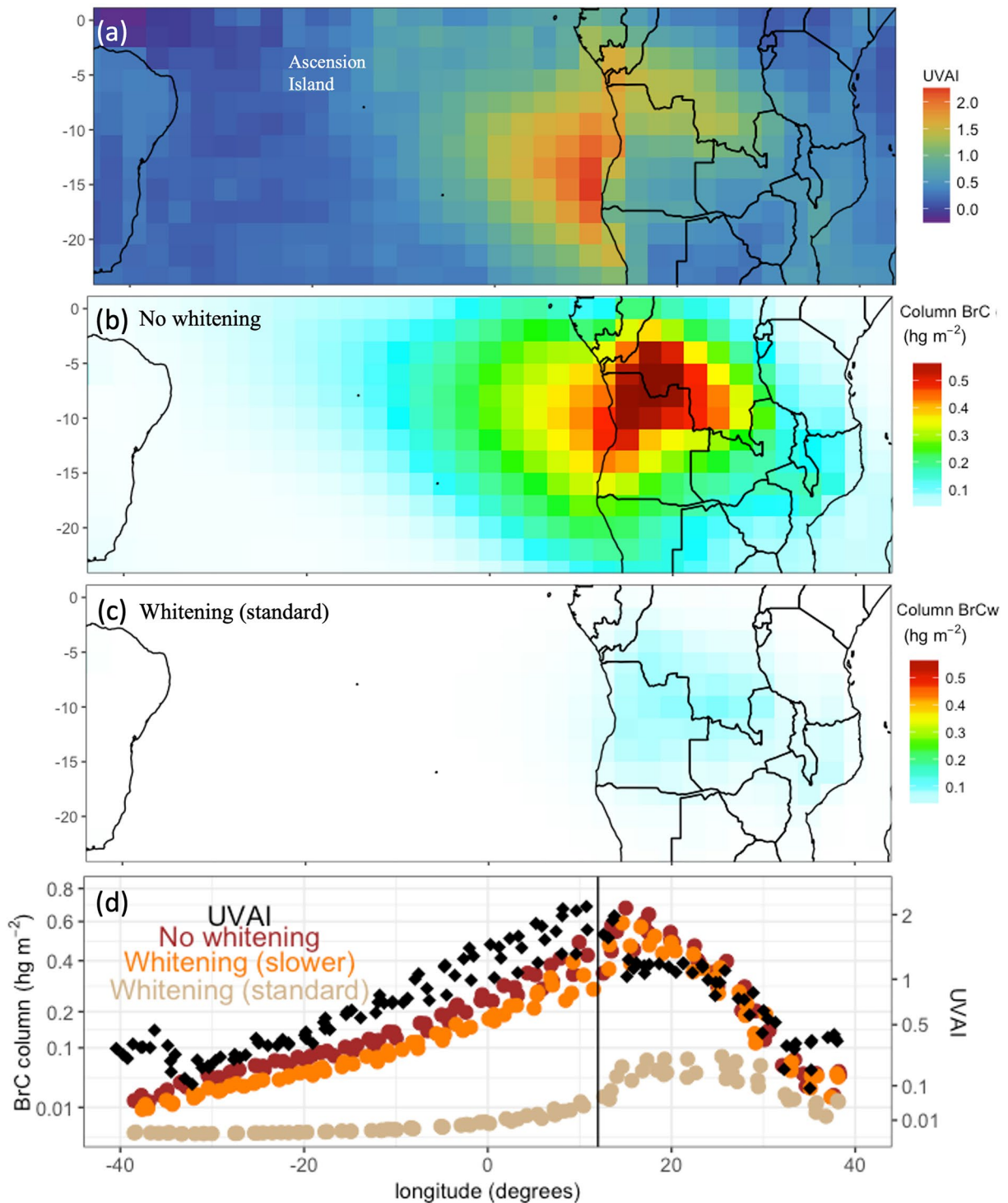


**Figure 9.** The mean August–September 2017 spatial distributions of the OMI UVAI (a), total simulated column burden of brown carbon (BrC) (b), and total simulated column burden of BrC with the baseline whitening scheme (c)—all at  $2^\circ \times 2.5^\circ$ . Column BrC is saturated at maximum values. Panel d shows column-integrated BrC concentrations averaged across August–September 2017 with our baseline BrC in red, our slower whitening lifetime simulation in orange, and our standard whitening scheme in beige within a box off the coast of southern Africa bounded by latitude =  $-12^\circ$  to  $-5^\circ$  and longitude =  $-40^\circ$ – $40^\circ$ . OMI UVAI observations for the same region are overlaid in black diamonds. A vertical line at  $12^\circ$  is the approximate edge of the African continent. The y axes have been transformed by a square-root function.

least partially, accounting for a neglected initial stage of BrC net enhancement after emission mentioned above in Section 4. However, we caution that these are qualitative comparisons. It is computationally intensive (and beyond the resources of this study) to repeat the detailed radiative calculations required to directly compare our simulations with the OMI UVAI product as done by Hammer et al. (2016, 2018). Coincident measurements of aerosol composition, size, and absorption within the export plume would be needed to directly constrain the evolution of BrC absorption.

We also investigate the global implications of the photochemical whitening of BrC (an optical loss process only and not a physical loss of BrC [e.g., fragmentation and evaporation]). The global burden of BrC without whitening (4.64 Tg) is a factor of three higher than with the 1-day whitening scheme (1.38 Tg) – OA mass is conserved; the whitened BrC is tracked separately as white POA. Correspondingly, we estimate an annual mean all-sky BrC DRE of  $+0.29 \text{ W m}^{-2}$ , which is reduced to  $+0.08 \text{ W m}^{-2}$  when including whitening using the 1-day whitening scheme (Figure 10). Both values fall within the (large) literature range ( $+0.03$  to  $+0.6 \text{ W m}^{-2}$ ) (Feng et al., 2013; Lin et al., 2014; Wang et al., 2014, 2018). Given the model underestimate of smoke concentrations downwind of Africa seen in Figure 5, these numbers are likely a lower limit. We calculate that the net effect of all BBA (BC:  $+0.05 \text{ W m}^{-2}$ , BrC given above (with 1-day whitening scheme, white POA:  $-0.10 \text{ W m}^{-2}$ ), and SOA:  $-0.05 \text{ W m}^{-2}$  from fires) on all-sky annual mean DRE, which switches from positive without whitening to slightly negative with whitening ( $+0.19 \text{ W m}^{-2}$  without whitening,  $-0.02 \text{ W m}^{-2}$  with whitening). This range suggests that the timescales for photochemical whitening of BrC could dictate a significant change in magnitude and possibly a change in the sign of the net DRE of BBA, highlighting the importance of better observational constraints on this process

## 6. Conclusions

Significant uncertainties exist around both the abundance and properties of BBA—our work investigates this in two major BB regions, the western United States and southern Africa, and explores the implications of this work globally. We show that BB BC is underestimated during ORACLES-2016 and CLARIFY, suggesting an underestimate in BB inventories in southern Africa, and that simulated anthropogenic BC is overestimated in the US when using the 2011 NEI. We address these biases through scaling of emission factors and filtering out of more anthropogenically influenced air masses, respectively. The resulting model is able to capture the large regional difference in observed BC:OA albeit with an underestimate of CLARIFY. Comparing modeled MAC with observations of absorption from each campaign, we show that our BC optical properties for smoke (which include an AE of 1.5 for BB BC) are generally consistent with observations at longer wavelengths (660 nm) during WE-CAN. However, more absorbing BC (achieved either via a higher baseline MAC [Forestieri et al., 2018; McClure et al., 2020] or a higher AE as in Taylor et al., 2020), would better capture measurements downwind of Africa. Our analysis of African outflow also suggests that the low bias in the model AAE of BC may contribute to the model underestimate of absorption at shorter wavelengths. We also show that an increase in BrC absorption can help explain these observations at short visible wavelengths.

Our comparisons of the measurements from WE-CAN and ORACLES-2016/CLARIFY demonstrate that African smoke (BC and/or BrC) is substantially more absorbing at shorter wavelengths than suggested by our baseline simulations. Brown et al. (2021) recently suggested that most models overestimate BB absorption, but their work focused on absorption at longer wavelengths (550 and 700 nm). More absorbing BrC downwind of Africa is consistent with a higher BC:OA ratio observed in African outflow and captured by our model simulations. We implement two parameterizations of BrC absorption based on the BC:OA ratio (McClure et al., 2020; Saleh et al., 2014). These schemes improve our ability to simulate the  $\text{MAC}_{\text{BC} + \text{OA}}$  at short wavelengths for fires downwind of Africa, but lead to an overestimate in absorption during WE-CAN when not invoking whitening. Thus, neither scheme sufficiently represents the considerably lower absorption of BrC in smoke from the western United States and the more absorbing BrC from African fires. One possible explanation is that Mie theory (used in Saleh et al.) may not be a good representation of optical properties for fresh smoke (Womack et al., 2020), as sampled during WE-CAN. Additional multi-wavelength measurements, with a focus on determination of BrC properties from primary BBOA when the BC:OA ratio  $<0.1$ , would be helpful in improving these parameterizations. McClure et al. (2020) showed

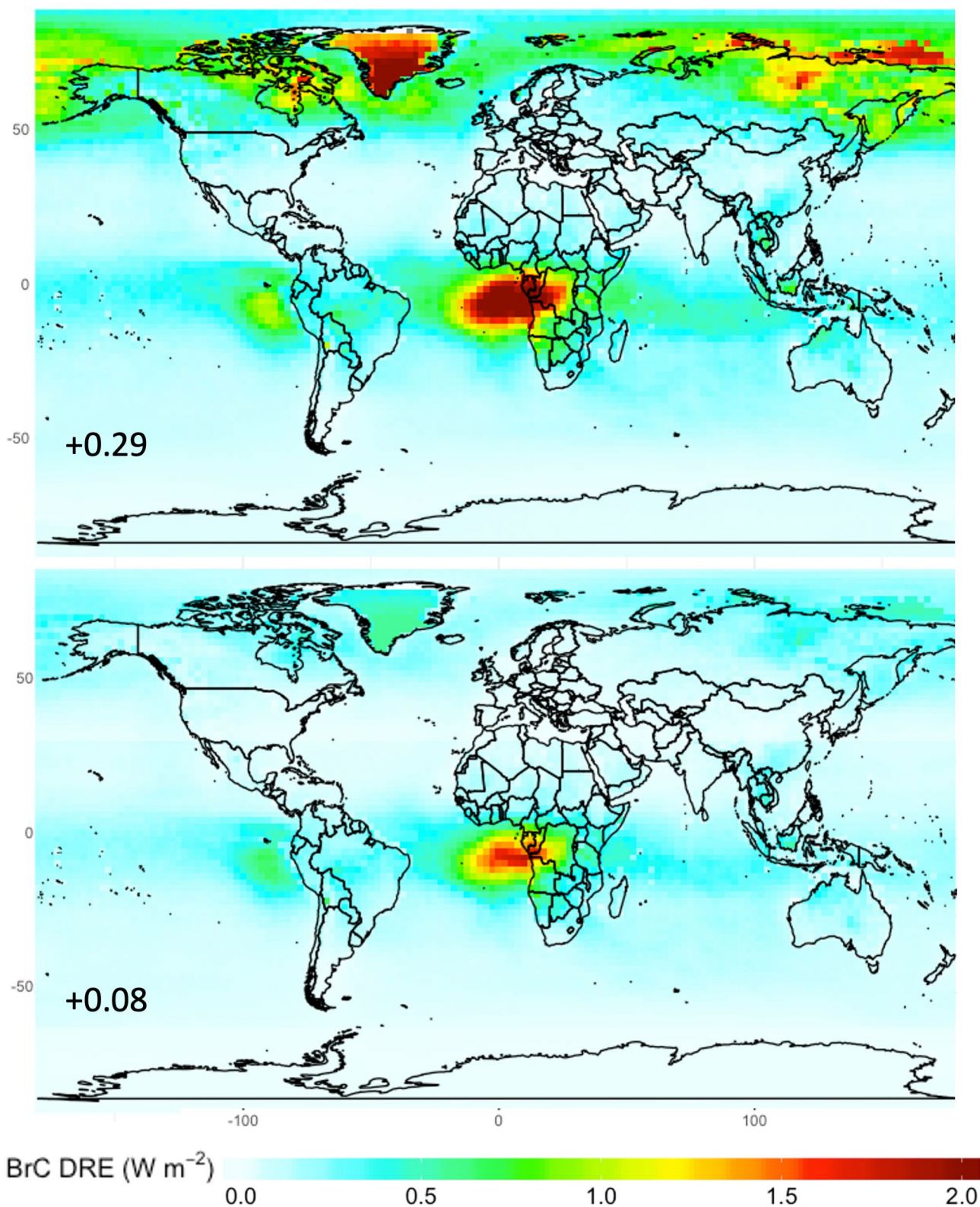


**Figure 10.** The global annual mean all-sky brown carbon direct radiative effect at the top of the atmosphere (TOA) in 2018 from a simulation without whitening (top) and when including whitening with a 1-day whitening scheme (bottom). Numbers indicate the global mean value in  $\text{W m}^{-2}$ .

that the uncertainty increases as the BC:OA ratio increases. Lab observations also suggest that there is some additional dependence on what is burned outside of a simple BC:OA paradigm. We also find that the FIREX parameterization enhances the absorption of BrC downwind of Africa at longer wavelengths, reducing the BC AE needed to explain observations during ORACLES and CLARIFY.

Our analysis relies on the contrast of total absorption measurements at two wavelengths in two different regions. This type of analysis is complicated by convolving the properties of various absorbers, the relevance of fixed assumptions for absorption efficiency, and the use of differing instrumentation across field campaigns. Absorption measurements at more than two wavelengths, and thus multiple AAE determinations, in different environments would offer additional opportunities to constrain models. More comprehensive field observations of the size of BC and BrC along with species-specific absorption measurements (e.g., BrC absorption measured directly from filter extracts, alongside total absorption measurements) at multiple wavelengths could better discern the relative contributions of BC and BrC.

This analysis provides qualitative evidence for the need to include whitening (on a 1-day timescale, or even faster) to capture observations from WE-CAN, but uncertainties in the baseline properties for BC and BrC from African fires make it more challenging to comment on the role of photochemical whitening during the ORACLES-2016 and CLARIFY campaigns. Our qualitative comparisons with the OMI UVAI in African outflows support a whitening timescale of 1 day or longer. These comparisons also suggest that linking the timescale of photobleaching to OH concentrations, as in our standard simulation, may not be appropriate, given the resulting very fast bleaching that would result in the tropics. It is possible that whitening timescales could vary regionally given that different fuel types produce distinct amounts of nitrogen-containing species, which have been associated with BrC (Mohr et al., 2013; Palm et al., 2020; Teich et al., 2017; Yuan et al., 2020). Analyses of WE-CAN show that there were large concentrations of N-containing species during the campaign (e.g.,  $[\text{NH}_3] > 50$  ppb in concentrated smoke plumes; Pollack et al., 2019) and suggest that nitroaromatics are important for BrC (Palm et al., 2020). However, no comparable measurements downwind of Africa exist to test whether the nitrogen content of smoke might dictate whitening timescales. More work is needed to determine the timescale of photochemical whitening in smoke from different fuels, whether OH concentrations or photolysis are controlling parameters, and how model resolution may affect these parameterizations.

Our comparison of smoke optical properties in two important, but very different, regions has implications for aerosol remote sensing algorithms. Typically, such retrievals assume constant properties, but the large differences in absorption shown here, as well as the dynamic properties associated with photochemical whitening, suggest that such an approach may introduce retrieval artifacts. Therefore, further refinement of BrC parameterizations may also help inform the development of remote sensing algorithms.

The global mean DRE of BrC is very sensitive to the timescale of photochemical whitening. This process may dictate the overall importance of the DRE from carbonaceous aerosol in smoke. Using our best estimate of a universal 1-day timescale for whitening (not dependent on OH), we find a global DRE of BBA of  $-0.02 \text{ W m}^{-2}$ , neglecting whitening results in a considerably more warming DRE for fires ( $+0.19 \text{ W m}^{-2}$ ). Additional observations in fire outflow, over long timescales, and from varying fuel types, are needed to better understand the magnitude and evolution of BrC absorption, and thus the global radiative impacts of smoke.

### Conflict of Interest

The authors declare no conflicts of interest relevant to this study.

### Data Availability Statement

The GEOS-Chem model is publicly available at: <https://doi.org/10.5281/zenodo.2620535> (GEOS-Chem, 2019). The IMPROVE data are also available publicly at: <http://vista.cira.colostate.edu/Improve/data-page/> (last access: February 24, 2020) (IMPROVE, 2020). The DC3 campaign data are available at [https://www.eol.ucar.edu/field\\_projects/dc3](https://www.eol.ucar.edu/field_projects/dc3) (last access: February 18, 2018) (NCAR, 2017), and the ARCTAS cam-

campaign data are available at: <https://www-air.larc.nasa.gov/cgi-bin/ArcView/arctas> (last access: February 18, 2018) (NASA, 2011). The WE-CAN campaign data are available at <https://www-air.larc.nasa.gov/cgi-bin/ArcView/firexaq?MERGE=1> (last access January 27, 2020) (NASA, 2020). The ORACLES campaign data are available at <https://espo.nasa.gov/oracles/archive/browse/oracles/id8/P3> (last access August 23, 2019) (NASA, 2019). The CLARIFY campaign data are available at <https://catalogue.ceda.ac.uk/uuid/38ab7089781a4560b067dd6c20af3769> (last access June 12, 2020) (FAAM, 2020).

### Acknowledgments

This research has been supported by the NOAA Climate Program Office, NA16OAR4310112 for T. S. Carter, C. L. Heald, and J. H. Kroll; NA16OAR4310111 for C. D. Cappa; and NA17OAR4310010 for L. A. Garofalo, E. J. T. Levin, D. K. Farmer and by NSF, #AGS-1650786 for E. J. T. Levin; #AGS-1650275 for L. Hu; and #AGS-1650493 for S. M. Murphy and R. P. Pokhrel. We acknowledge the Natural Environmental Research Council (NERC) (grant NE/L013479/1) for funding the measurements performed during CLARIFY-2017. We thank everyone involved in the planning and execution of the CLARIFY-2017 project. The BAe-146-301 atmospheric research aircraft was flown by Airtask and managed by the Facility for Airborne Atmospheric Measurements (FAAM), which is a joint entity of NERC and the Met Office. The authors thank Armin Wisthaler and Tomas Mikoviny for acetonitrile measurements from both ARCTAS and DC3, Wade Permar for acetonitrile measurements during WE-CAN, and Paul DeMott and Sonia Kreidenweis for carbonaceous aerosol mass concentration measurements during WE-CAN. We thank James Podolske and Steven Howell for measurements during ORACLES. We acknowledge data from the IMPROVE network. IMPROVE is a collaborative association of state, tribal, and federal agencies and international partners. The US Environmental Protection Agency is the primary funding source, with contracting and research support from the National Park Service. The Air Quality Group at the University of California, Davis, is the central analytical laboratory, with ion analysis provided by Research Triangle Institute and carbon analysis provided by Desert Research Institute.

### References

- Akagi, S., Yokelson, R., Wiedinmyer, C., Alvarado, M., Reid, J., Karl, T., et al. (2011). Emission factors for open and domestic biomass burning for use in atmospheric models. *Atmospheric Chemistry and Physics*, *11*, 4039–4072.
- Andela, N., Morton, D. C., Giglio, L., Chen, Y., Werf, G. R. v. d., Kasibhatla, P. S., et al. (2017). A human-driven decline in global burned area. *Science*, *356*(6345), 1356–1362. <https://doi.org/10.1126/science.aal4108>
- Andreae, M. O. (2019). Emission of trace gases and aerosols from biomass burning—An updated assessment. *Atmospheric Chemistry and Physics*, *19*(13), 8523–8546. <https://doi.org/10.5194/acp-19-8523-2019>
- Aruffo, E., Biancofiore, F., Di Carlo, P., Busilacchio, M., Verdecchia, M., Tomassetti, B., et al. (2016). Impact of biomass burning emission on total peroxy nitrates: Fire plume identification during the BORTAS campaign. *Atmospheric Measurement Techniques*, *9*(11), 5591–5606. <https://doi.org/10.5194/amt-9-5591-2016>
- Bond, T. C., Anderson, T. L., & Campbell, D. (1999). Calibration and Intercomparison of filter-based measurements of visible light absorption by aerosols. *Aerosol Science and Technology*, *30*(6), 582–600. <https://doi.org/10.1080/027868299304435>
- Bond, T. C., & Bergstrom, R. W. (2006). Light absorption by carbonaceous particles: An investigative review. *Aerosol Science and Technology*, *40*(1), 27–67. <https://doi.org/10.1080/02786820500421521>
- Bond, T. C., Doherty, S. J., Fahey, D. W., Forster, P. M., Berntsen, T., DeAngelo, B. J., et al. (2013). Bounding the role of black carbon in the climate system: A scientific assessment. *Journal of Geophysical Research: Atmospheres*, *118*(11), 5380–5552. <https://doi.org/10.1002/jgrd.50171>
- Bond, T. C., Habib, G., & Bergstrom, R. W. (2006). Limitations in the enhancement of visible light absorption due to mixing state. *Journal of Geophysical Research*, *111*, D20211. <https://doi.org/10.1029/2006JD007315>
- Brown, H., Liu, X., Pokhrel, R., Murphy, S., Lu, Z., Saleh, R., et al. (2021). Biomass burning aerosols in most climate models are too absorbing. *Nature Communications*, *12*(1), 277. <https://doi.org/10.1038/s41467-020-20482-9>
- Cappa, C. D., Lim, C. Y., Hagan, D. H., Coggon, M., Koss, A., Sekimoto, K., et al. (2020). Biomass-burning-derived particles from a wide variety of fuels—Part 2: Effects of photochemical aging on particle optical and chemical properties. *Atmospheric Chemistry and Physics*, *20*(14), 8511–8532. <https://doi.org/10.5194/acp-20-8511-2020>
- Cappa, C. D., Onasch, T. B., Massoli, P., Worsnop, D. R., Bates, T. S., Cross, E. S., et al. (2012). Radiative absorption enhancements due to the mixing state of atmospheric black carbon. *Science*, *337*(6098), 1078–1081. <https://doi.org/10.1126/science.1223447>
- Carter, T. S., Heald, C. L., Jimenez, J. L., Campuzano-Jost, P., Kondo, Y., Moteki, N., et al. (2020). How emissions uncertainty influences the distribution and radiative impacts of smoke from fires in North America. *Atmospheric Chemistry and Physics*, *20*, 2073–2097. <https://doi.org/10.5194/acp-20-2073-2020>
- Chan Miller, C., Jacob, D. J., Marais, E. A., Yu, K., Travis, K. R., Kim, P. S., et al. (2017). Glyoxal yield from isoprene oxidation and relation to formaldehyde: Chemical mechanism, constraints from SENEX aircraft observations, and interpretation of OMI satellite data. *Atmospheric Chemistry and Physics*, *17*(14), 8725–8738. <https://doi.org/10.5194/acp-17-8725-2017>
- Chin, M., Ginoux, P., Kinne, S., Torres, O., Holben, B. N., Duncan, B. N., et al. (2002). Tropospheric aerosol optical thickness from the GO-CART model and comparisons with satellite and sun photometer measurements. *Journal of the Atmospheric Sciences*, *59*(3), 461–483. [https://doi.org/10.1175/1520-0469\(2002\)059<0461:TAOTFT>2.0.CO;2](https://doi.org/10.1175/1520-0469(2002)059<0461:TAOTFT>2.0.CO;2)
- Chow, J. C., Watson, J. G., Chen, L.-W. A., Chang, M. C. O., Robinson, N. F., Trimble, D., & Kohl, S. (2007). The IMPROVE\_A temperature protocol for thermal/optical carbon analysis: Maintaining consistency with a long-term database. *Journal of the Air & Waste Management Association*, *57*(9), 1014–1023. <https://doi.org/10.3155/1047-3289.57.9.1014>
- Chung, C. E., Ramanathan, V., & Decremier, D. (2012). Observationally constrained estimates of carbonaceous aerosol radiative forcing. *Proceedings of the National Academy of Sciences*, *109*(29), 11624–11629. <https://doi.org/10.1073/pnas.1203707109>
- Cooke, W. F., Liousse, C., Cachier, H., & Feichter, J. (1999). Construction of a 1° × 1° fossil fuel emission data set for carbonaceous aerosol and implementation and radiative impact in the ECHAM4 model. *Journal of Geophysical Research*, *104*(D18), 22137–22162. <https://doi.org/10.1029/1999JD900187>
- Cotterell, M. I., Szpek, K., Haywood, J. M., & Langridge, J. M. (2020). Sensitivity and accuracy of refractive index retrievals from measured extinction and absorption cross sections for mobility-selected internally mixed light absorbing aerosols. *Aerosol Science and Technology*, *54*(9), 1034–1057. <https://doi.org/10.1080/02786826.2020.1757034>
- Cotterell, M. I., Szpek, K., Tiddeman, D. A., Haywood, J. M., & Langridge, J. M. (2021). Photoacoustic studies of energy transfer from ozone photoproducts to bath gases following Chappuis band photoexcitation. *Physical Chemistry Chemical Physics*, *23*(1), 536–553. <https://doi.org/10.1039/D0CP05056C>
- Das, S., Harshvardhan, H., Bian, H., Chin, M., Curci, G., Protonotariou, A. P., et al. (2017). Biomass burning aerosol transport and vertical distribution over the South African-Atlantic region. *Journal of Geophysical Research: Atmospheres*, *122*(12), 6391–6415. <https://doi.org/10.1002/2016JD026421>
- Davies, N. W., Cotterell, M. I., Fox, C., Szpek, K., Haywood, J. M., & Langridge, J. M. (2018). On the accuracy of aerosol photoacoustic spectrometer calibrations using absorption by ozone. *Atmospheric Measurement Techniques*, *11*(4), 2313–2324. <https://doi.org/10.5194/amt-11-2313-2018>
- Davies, N. W., Fox, C., Szpek, K., Cotterell, M. I., Taylor, J. W., Allan, J. D., et al. (2019). Evaluating biases in filter-based aerosol absorption measurements using photoacoustic spectroscopy. *Atmospheric Measurement Techniques*, *12*(6), 3417–3434. <https://doi.org/10.5194/amt-12-3417-2019>



- Denjean, C., Bourrienne, T., Burnet, F., Mallet, M., Maury, N., Colomb, A., et al. (2020). Overview of aerosol optical properties over southern West Africa from DACCIWA aircraft measurements. *Atmospheric Chemistry and Physics*, 20(8), 4735–4756. <https://doi.org/10.5194/acp-20-4735-2020>
- Drury, E., Jacob, D. J., Spurr, R. J. D., Wang, J., Shinzuka, Y., Anderson, B. E., et al. (2010). Synthesis of satellite (MODIS), aircraft (ICARTT), and surface (IMPROVE, EPA-AQS, AERONET) aerosol observations over eastern North America to improve MODIS aerosol retrievals and constrain surface aerosol concentrations and sources. *Journal of Geophysical Research*, 115(D14). <https://doi.org/10.1029/2009JD012629>
- Eastham, S. D., & Jacob, D. J. (2017). Limits on the ability of global Eulerian models to resolve intercontinental transport of chemical plumes. *Atmospheric Chemistry and Physics*, 17(4), 2543–2553. <https://doi.org/10.5194/acp-17-2543-2017>
- Feng, Y., Ramanathan, V., & Kotamarthi, V. R. (2013). Brown carbon: A significant atmospheric absorber of solar radiation? *Atmospheric Chemistry and Physics*, 13(17), 8607–8621. <https://doi.org/10.5194/acp-13-8607-2013>
- Fischer, E. V., Jacob, D. J., Yantosca, R. M., Sulprizio, M. P., Millet, D. B., Mao, J., et al. (2014). Atmospheric peroxyacetyl nitrate (PAN): A global budget and source attribution. *Atmospheric Chemistry and Physics*, 14(5), 2679–2698. <https://doi.org/10.5194/acp-14-2679-2014>
- Ford, B., Martin, M. V., Zelasky, S. E., Fischer, E. V., Anenberg, S. C., Heald, C. L., & Pierce, J. R. (2018). Future fire impacts on smoke concentrations, visibility, and health in the contiguous United States. *GeoHealth*, 2(8), 229–247. <https://doi.org/10.1029/2018GH000144>
- Forestieri, S. D., Staudt, S. M., Kuborn, T. M., Faber, K., Ruehl, C. R., Bertram, T. H., & Cappa, C. D. (2018). Establishing the impact of model surfactants on cloud condensation nuclei activity of sea spray aerosol mimics. *Atmospheric Chemistry and Physics*, 18(15), 10985–11005. <https://doi.org/10.5194/acp-18-10985-2018>
- Forrister, H., Liu, J., Scheuer, E., Dibb, J., Ziemba, L., Thornhill, K. L., et al. (2015). Evolution of brown carbon in wildfire plumes. *Geophysical Research Letters*, 42(11), 4623–4630. <https://doi.org/10.1002/2015GL063897>
- Foster, K., Pokhrel, R., Burkhart, M., & Murphy, S. (2019). A novel approach to calibrating a photoacoustic absorption spectrometer using polydisperse absorbing aerosol. *Atmospheric Measurement Techniques*, 12(6), 3351–3363. <https://doi.org/10.5194/amt-12-3351-2019>
- Fountoukis, C., & Nenes, A. (2007). ISORROPIA II: A computationally efficient thermodynamic equilibrium model for  $K^+$ - $Ca^{2+}$ - $Mg^{2+}$ - $NH_4^+$ - $Na^+$ - $SO_4^{2-}$ - $NO_3^-$ - $Cl^-$ - $H_2O$  aerosols. *Atmospheric Chemistry and Physics*, 48.
- Fuller, K. A., Malm, W. C., & Kreidenweis, S. M. (1999). Effects of mixing on extinction by carbonaceous particles. *Journal of Geophysical Research*, 104(D13), 15941–15954. <https://doi.org/10.1029/1998JD100069>
- Garofalo, L. A., Pothier, M. A., Levin, E. J. T., Campos, T., Kreidenweis, S. M., & Farmer, D. K. (2019). Emission and evolution of submicron organic aerosol in smoke from wildfires in the western United States. *ACS Earth and Space Chemistry*, 3(7), 1237–1247. <https://doi.org/10.1021/acsearthspacechem.9b00125>
- Giglio, L., Boschetti, L., Roy, D. P., Humber, M. L., & Justice, C. O. (2018). The Collection 6 MODIS burned area mapping algorithm and product. *Remote Sensing of Environment*, 217, 72–85. <https://doi.org/10.1016/j.rse.2018.08.005>
- Guenther, A. B., Jiang, X., Heald, C. L., Sakulyanontvittaya, T., Duhl, T., Emmons, L. K., & Wang, X. (2012). The Model of Emissions of Gases and Aerosols from Nature version 2.1 (MEGAN2.1): An extended and updated framework for modeling biogenic emissions. *Geoscientific Model Development*, 5(6), 1471–1492. <https://doi.org/10.5194/gmd-5-1471-2012>
- Hammer, M. S., Martin, R. V., Li, C., Torres, O., Manning, M., & Boys, B. L. (2018). Insight into global trends in aerosol composition from 2005 to 2015 inferred from the OMI Ultraviolet Aerosol Index. *Atmospheric Chemistry and Physics*, 18(11), 8097–8112. <https://doi.org/10.5194/acp-18-8097-2018>
- Hammer, M. S., Martin, R. V., van Donkelaar, A., Buchard, V., Torres, O., Ridley, D. A., & Spurr, R. J. D. (2016). Interpreting the ultraviolet aerosol index observed with the OMI satellite instrument to understand absorption by organic aerosols: Implications for atmospheric oxidation and direct radiative effects. *Atmospheric Chemistry and Physics*, 16(4), 2507–2523. <https://doi.org/10.5194/acp-16-2507-2016>
- Hansen, A. D. A., Rosen, H., & Novakov, T. (1983). *Aethalometer—An instrument for the real-time measurement of optical absorption by aerosol particles (LBL-16106; CONF-8309166-1)*. Lawrence Berkeley Lab. Retrieved from <https://www.osti.gov/biblio/5535057>
- Haslett, S. L., Taylor, J. W., Evans, M., Morris, E., Vogel, B., Dajuma, A., et al. (2019). Remote biomass burning dominates southern West African air pollution during the monsoon. *Atmospheric Chemistry and Physics*, 19(24), 15217–15234. <https://doi.org/10.5194/acp-19-15217-2019>
- Haywood, J. M., Abel, S. J., Barrett, P. A., Bellouin, N., Blyth, A., Bower, K. N., et al. (2021). The CLOUD–Aerosol–Radiation Interaction and Forcing: Year 2017 (CLARIFY-2017) measurement campaign. *Atmospheric Chemistry and Physics*, 21(2), 1049–1084. <https://doi.org/10.5194/acp-21-1049-2021>
- Heald, C. L., Ridley, D. A., Kroll, J. H., Barrett, S. R. H., Cady-Pereira, K. E., Alvarado, M. J., & Holmes, C. D. (2014). Contrasting the direct radiative effect and direct radiative forcing of aerosols. *Atmospheric Chemistry and Physics*, 14(11), 5513–5527. <https://doi.org/10.5194/acp-14-5513-2014>
- Hoelsy, R. M., Smith, S. J., Feng, L., Klimont, Z., Janssens-Maenhout, G., Pitkanen, T., et al. (2018). Historical (1750–2014) anthropogenic emissions of reactive gases and aerosols from the Community Emissions Data System (CEDS). *Geoscientific Model Development*, 11(1), 369–408. <https://doi.org/10.5194/gmd-11-369-2018>
- Iacono, M. J., Delamere, J. S., Mlawer, E. J., Shephard, M. W., Clough, S. A., & Collins, W. D. (2008). Radiative forcing by long-lived greenhouse gases: Calculations with the AER radiative transfer models. *Journal of Geophysical Research: Atmospheres*, 113(D13). <https://doi.org/10.1029/2008JD009944>
- Ichoku, C. (2020). African biomass burning and its atmospheric impacts. *Oxford Research Encyclopedia of Climate Science*. <https://doi.org/10.1093/acrefore/9780190228620.013.523>
- Intergovernmental Panel on Climate Change. (2014). *AR5 synthesis report: Climate change 2014—IPCC*. Retrieved from <https://www.ipcc.ch/report/ar5/syr/>
- Jacobson, M. Z. (2000). A physically-based treatment of elemental carbon optics: Implications for global direct forcing of aerosols. *Geophysical Research Letters*, 27(2), 217–220. <https://doi.org/10.1029/1999GL010968>
- Jo, D. S., Park, R. J., Lee, S., Kim, S.-W., & Zhang, X. (2016). A global simulation of brown carbon: Implications for photochemistry and direct radiative effect. *Atmospheric Chemistry and Physics*, 16(5), 3413–3432. <https://doi.org/10.5194/acp-16-3413-2016>
- Johnston, F. H., Henderson Sarah, B., Yang, C., Randerson James, T., Miriam, M., DeFries Ruth, S., et al. (2012). Estimated global mortality attributable to smoke from landscape fires. *Environmental Health Perspectives*, 120(5), 695–701. <https://doi.org/10.1289/ehp.1104422>
- Jones, B. A. (2017). Are we underestimating the economic costs of wildfire smoke? An investigation using the life satisfaction approach. *Journal of Forest Economics*, 27, 80–90. <https://doi.org/10.1016/j.jfe.2017.03.004>
- Kahnert, M., & Kanngießner, F. (2020). Modeling optical properties of atmospheric black carbon aerosols. *Journal of Quantitative Spectroscopy and Radiative Transfer*, 244, 106849. <https://doi.org/10.1016/j.jqsrt.2020.106849>

- Kim, P. S., Jacob, D. J., Fisher, J. A., Travis, K., Yu, K., Zhu, L., et al. (2015). Sources, seasonality, and trends of southeast US aerosol: An integrated analysis of surface, aircraft, and satellite observations with the GEOS-Chem chemical transport model. *Atmospheric Chemistry and Physics*, *15*(18), 10411–10433. <https://doi.org/10.5194/acp-15-10411-2015>
- Ko, J., Krasowsky, T., & Ban-Weiss, G. (2020). Measurements to determine the mixing state of black carbon emitted from the 2017–2018 California wildfires and urban Los Angeles. *Atmospheric Chemistry and Physics*, *20*(24), 15635–15664. <https://doi.org/10.5194/acp-20-15635-2020>
- Köpke, P., Hess, M., Schult, I., & Shettle, E. P. (1997). *Global aerosol data set*. Max-Planck-Inst. für Meteorologie.
- Lack, D. A., Cappa, C. D., Covert, D. S., Baynard, T., Massoli, P., Sierau, B., et al. (2008). Bias in filter-based aerosol light absorption measurements due to organic aerosol loading: Evidence from ambient measurements. *Aerosol Science and Technology*, *42*(12), 1033–1041. <https://doi.org/10.1080/02786820802389277>
- Lack, D. A., Langridge, J. M., Bahreini, R., Cappa, C. D., Middlebrook, A. M., & Schwarz, J. P. (2012). Brown carbon and internal mixing in biomass burning particles. *Proceedings of the National Academy of Sciences*, *109*(37), 14802–14807. <https://doi.org/10.1073/pnas.1206575109>
- Laskin, A., Laskin, J., & Nizkorodov, S. A. (2015). Chemistry of atmospheric brown carbon. *Chemical Reviews*, *115*(10), 4335–4382. <https://doi.org/10.1021/cr5006167>
- Lin, G., Penner, J. E., Flanner, M. G., Sillman, S., Xu, L., & Zhou, C. (2014). Radiative forcing of organic aerosol in the atmosphere and on snow: Effects of SOA and brown carbon. *Journal of Geophysical Research: Atmospheres*, *119*(12), 7453–7476. <https://doi.org/10.1002/2013JD021186>
- Liu, D., He, C., Schwarz, J. P., & Wang, X. (2020). Lifecycle of light-absorbing carbonaceous aerosols in the atmosphere. *Npj Climate and Atmospheric Science*, *3*(1), 1–18. <https://doi.org/10.1038/s41612-020-00145-8>
- Liu, J. C., Pereira, G., Uhl, S. A., Bravo, M. A., & Bell, M. L. (2015). A systematic review of the physical health impacts from non-occupational exposure to wildfire smoke. *Environmental Research*, *136*, 120–132. <https://doi.org/10.1016/j.envres.2014.10.015>
- Luo, G., Yu, F., & Schwab, J. (2019). Revised treatment of wet scavenging processes dramatically improves GEOS-Chem 12.0.0 simulations of surface nitric acid, nitrate, and ammonium over the United States. *Geoscientific Model Development*, *12*(8), 3439–3447. <https://doi.org/10.5194/gmd-12-3439-2019>
- Mao, J., Paulot, F., Jacob, D. J., Cohen, R. C., Crounse, J. D., Wennberg, P. O., et al. (2013). Ozone and organic nitrates over the eastern United States: Sensitivity to isoprene chemistry. *Journal of Geophysical Research: Atmospheres*, *118*(19), 11256–11268. <https://doi.org/10.1002/jgrd.50817>
- Marais, E. A., & Wiedinmyer, C. (2016). Air quality impact of Diffuse and Inefficient Combustion Emissions in Africa (DICE-Africa). *Environmental Science & Technology*, *50*(19), 10739–10745. <https://doi.org/10.1021/acs.est.6b02602>
- McClure, C. D., Lim, C. Y., Hagan, D. H., Kroll, J. H., & Cappa, C. D. (2020). Biomass-burning-derived particles from a wide variety of fuels & #8211; Part 1: Properties of primary particles. *Atmospheric Chemistry and Physics*, *20*(3), 1531–1547. <https://doi.org/10.5194/acp-20-1531-2020>
- McMeeking, G. R., Fortner, E., Onasch, T. B., Taylor, J. W., Flynn, M., Coe, H., & Kreidenweis, S. M. (2014). Impacts of nonrefractory material on light absorption by aerosols emitted from biomass burning. *Journal of Geophysical Research: Atmospheres*, *119*(21), 12272–12286. <https://doi.org/10.1002/2014JD021750>
- Moffet, R. C., & Prather, K. A. (2009). In-situ measurements of the mixing state and optical properties of soot with implications for radiative forcing estimates. *Proceedings of the National Academy of Sciences*, *106*(29), 11872–11877. <https://doi.org/10.1073/pnas.0900040106>
- Mohr, C., Lopez-Hilfiker, F. D., Zotter, P., Prévôt, A. S. H., Xu, L., Ng, N. L., et al. (2013). Contribution of nitrated phenols to wood burning brown carbon light absorption in Detling, United Kingdom during Winter time. *Environmental Science & Technology*, *47*(12), 6316–6324. <https://doi.org/10.1021/es400683v>
- Müller, M., Mikoviny, T., Feil, S., Haidacher, S., Hanel, G., Hartungen, E., et al. (2014). A compact PTR-ToF-MS instrument for airborne measurements of volatile organic compounds at high spatiotemporal resolution. *Atmospheric Measurement Techniques*, *7*(11), 3763–3772. <https://doi.org/10.5194/amt-7-3763-2014>
- O'Dell, K., Hornbrook, R. S., Permar, W., Levin, E. J. T., Garofalo, L. A., Apel, E. C., et al. (2020). Hazardous air pollutants in fresh and aged western US wildfire smoke and implications for long-term exposure. *Environmental Science & Technology*, *54*(19), 11838–11847. <https://doi.org/10.1021/acs.est.0c04497>
- Ogren, J. A., Wendell, J., Andrews, E., & Sheridan, P. J. (2017). Continuous light absorption photometer for long-term studies. *Atmospheric Measurement Techniques*, *10*(12), 4805–4818. <https://doi.org/10.5194/amt-10-4805-2017>
- OMI Team. (2012). *Ozone monitoring instrument (OMI) data user's guide*. Retrieved from [https://docserver.gesdisc.eosdis.nasa.gov/repository/Mission/OMI/3.3\\_ScienceDataProductDocumentation/3.3.2\\_ProductRequirements\\_Designs/README.OMI\\_DUG.pdf](https://docserver.gesdisc.eosdis.nasa.gov/repository/Mission/OMI/3.3_ScienceDataProductDocumentation/3.3.2_ProductRequirements_Designs/README.OMI_DUG.pdf)
- Pai, S. J., Heald, C. L., Pierce, J. R., Farina, S. C., Marais, E. A., Jimenez, J. L., et al. (2020). An evaluation of global organic aerosol schemes using airborne observations. *Atmospheric Chemistry and Physics*, *20*(5), 2637–2665. <https://doi.org/10.5194/acp-20-2637-2020>
- Palm, B. B., Peng, Q., Fredrickson, C. D., Lee, B. H., Garofalo, L. A., Pothier, M. A., et al. (2020). Quantification of organic aerosol and brown carbon evolution in fresh wildfire plumes. *Proceedings of the National Academy of Sciences*, *117*, 202012218. <https://doi.org/10.1073/pnas.2012218117>
- Park, R. J., Jacob, D. J., Chin, M., & Martin, R. V. (2003). Sources of carbonaceous aerosols over the United States and implications for natural visibility. *Journal of Geophysical Research*, *108*(D12). <https://doi.org/10.1029/2002JD003190>
- Park, R. J., Kim, M. J., Jeong, J. I., Youn, D., & Kim, S. (2010). A contribution of brown carbon aerosol to the aerosol light absorption and its radiative forcing in East Asia. *Atmospheric Environment*, *44*(11), 1414–1421. <https://doi.org/10.1016/j.atmosenv.2010.01.042>
- Permar, W. Q., Wang, Q., Selimovic, V., Wielgasz, C., Yokelson, R. J., Hornbrook, R. S., et al. (2021). Emissions of trace organic gases from western U.S. wildfires based on WE-CAN aircraft measurements. *Journal of Geophysical Research*, *126*, e2020JD033838. <https://doi.org/10.1029/2020JD033838>
- Perring, A. E., Schwarz, J. P., Markovic, M. Z., Fahey, D. W., Jimenez, J. L., Campuzano-Jost, P., et al. (2017). In situ measurements of water uptake by black carbon-containing aerosol in wildfire plumes. *Journal of Geophysical Research: Atmospheres*, *122*(2), 1086–1097. <https://doi.org/10.1002/2016JD025688>
- Phillip, S., Martin, R. V., & Keller, C. A. (2016). Sensitivity of chemistry-transport model simulations to the duration of chemical and transport operators: A case study with GEOS-Chem v10-01. *Geoscientific Model Development*, *9*(5), 1683–1695. <https://doi.org/10.5194/gmd-9-1683-2016>
- Pistone, K., Redemann, J., Doherty, S., Zuidema, P., Burton, S., Cairns, B., et al. (2019). Intercomparison of biomass burning aerosol optical properties from in situ and remote-sensing instruments in ORACLES-2016. *Atmospheric Chemistry and Physics*, *19*(14), 9181–9208. <https://doi.org/10.5194/acp-19-9181-2019>

- Pokhrel, R. P., Beamesderfer, E. R., Wagner, N. L., Langridge, J. M., Lack, D. A., Jayarathne, T., et al. (2017). Relative importance of black carbon, brown carbon, and absorption enhancement from clear coatings in biomass burning emissions. *Atmospheric Chemistry and Physics*, 17(8), 5063–5078. <https://doi.org/10.5194/acp-17-5063-2017>
- Pollack, I. B., Lindaas, J., Roscioli, J. R., Agnese, M., Permar, W., Hu, L., & Fischer, E. V. (2019). Evaluation of ambient ammonia measurements from a research aircraft using a closed-path QC-TILDAS operated with active continuous passivation. *Atmospheric Measurement Techniques*, 26.
- Ramo, R., Roteta, E., Bistinas, I., Wees, D. V., Bastarrika, A., Chuvieco, E., & van der Werf, G. R. (2021). African burned area and fire carbon emissions are strongly impacted by small fires undetected by coarse resolution satellite data. *Proceedings of the National Academy of Sciences*, 118(9). <https://doi.org/10.1073/pnas.2011160118>
- Rap, A., Scott, C. E., Spracklen, D. V., Bellouin, N., Forster, P. M., Carslaw, K. S., et al. (2013). Natural aerosol direct and indirect radiative effects. *Geophysical Research Letters*, 40(12), 3297–3301. <https://doi.org/10.1002/grl.50441>
- Rastigejev, Y., Park, R., Brenner, M. P., & Jacob, D. J. (2010). Resolving intercontinental pollution plumes in global models of atmospheric transport. *Journal of Geophysical Research*, 115(D2). <https://doi.org/10.1029/2009JD012568>
- Reid, C. E., Brauer, M., Johnston Fay, H., Jerrett Michael, Balmes John, R., & Elliott Catherine, T. (2016). Critical review of health impacts of wildfire smoke exposure. *Environmental Health Perspectives*, 124(9), 1334–1343. <https://doi.org/10.1289/ehp.1409277>
- Saleh, R., Robinson, E. S., Tkacik, D. S., Ahern, A. T., Liu, S., Aiken, A. C., et al. (2014). Brownness of organics in aerosols from biomass burning linked to their black carbon content. *Nature Geoscience*, 7(9), 647–650. <https://doi.org/10.1038/ngeo2220>
- Schwarz, J. P., Gao, R. S., Spackman, J. R., Watts, L. A., Thomson, D. S., Fahey, D. W., et al. (2008). Measurement of the mixing state, mass, and optical size of individual black carbon particles in urban and biomass burning emissions. *Geophysical Research Letters*, 35(13). <https://doi.org/10.1029/2008GL033968>
- Schwarz, J. P., Spackman, J. R., Fahey, D. W., Gao, R. S., Lohmann, U., Stier, P., et al. (2008). Coatings and their enhancement of black carbon light absorption in the tropical atmosphere. *Journal of Geophysical Research*, 113(D3). <https://doi.org/10.1029/2007JD009042>
- Sherwen, T., Schmidt, J. A., Evans, M. J., Carpenter, L. J., Großmann, K., Eastham, S. D., et al. (2016). Global impacts of tropospheric halogens (Cl, Br, I) on oxidants and composition in GEOS-Chem. *Atmospheric Chemistry and Physics*, 16(18), 12239–12271. <https://doi.org/10.5194/acp-16-12239-2016>
- Shinozuka, Y., Saide, P. E., Ferrada, G. A., Burton, S. P., Ferrare, R., Doherty, S. J., et al. (2019). Modeling the smoky troposphere of the southeast Atlantic: A comparison to ORACLES airborne observations from September of 2016. *Atmospheric Chemistry and Physics Discussions*, 1–77. <https://doi.org/10.5194/acp-2019-678>
- Shinozuka, Y., Saide, P. E., Ferrada, G. A., Burton, S. P., Ferrare, R., Doherty, S. J., et al. (2020). Modeling the smoky troposphere of the southeast Atlantic: A comparison to ORACLES airborne observations from September of 2016. *Atmospheric Chemistry and Physics*, 20(19), 11491–11526. <https://doi.org/10.5194/acp-20-11491-2020>
- Simone, N. W., Stettler, M. E. J., & Barrett, S. R. H. (2013). Rapid estimation of global civil aviation emissions with uncertainty quantification. *Transportation Research Part D: Transport and Environment*, 25, 33–41. <https://doi.org/10.1016/j.trd.2013.07.001>
- Stettler, M. E. J., Eastham, S., & Barrett, S. R. H. (2011). Air quality and public health impacts of UK airports. Part I: Emissions. *Atmospheric Environment*, 45(31), 5415–5424. <https://doi.org/10.1016/j.atmosenv.2011.07.012>
- Taylor, J. W., Wu, H., Szpek, K., Bower, K., Crawford, I., Flynn, M. J., et al. (2020). Absorption closure in highly aged biomass burning smoke. *Atmospheric Chemistry and Physics*, 20(19), 11201–11221. <https://doi.org/10.5194/acp-20-11201-2020>
- Teich, M., van Pinxteren, D., Wang, M., Kecorius, S., Wang, Z., Müller, T., et al. (2017). Contributions of nitrated aromatic compounds to the light absorption of water-soluble and particulate brown carbon in different atmospheric environments in Germany and China. *Atmospheric Chemistry and Physics*, 17(3), 1653–1672. <https://doi.org/10.5194/acp-17-1653-2017>
- Travis, K. R., Jacob, D. J., Fisher, J. A., Kim, P. S., Marais, E. A., Zhu, L., et al. (2016). Why do models overestimate surface ozone in the Southeastern United States? *Atmospheric Chemistry and Physics*, 16(21), 13561–13577. <https://doi.org/10.5194/acp-16-13561-2016>
- US EPA. (2015). *Air pollutant emissions trends data [policies and guidance]*. US EPA. Retrieved from <https://www.epa.gov/air-emissions-inventories/air-pollutant-emissions-trends-data>
- Val Martin, M., Heald, C. L., Lamarque, J.-F., Tilmes, S., Emmons, L. K., & Schichtel, B. A. (2015). How emissions, climate, and land use change will impact mid-century air quality over the United States: A focus on effects at national parks. *Atmospheric Chemistry and Physics*, 15(5), 2805–2823. <https://doi.org/10.5194/acp-15-2805-2015>
- van der Werf, G. R., Randerson, J. T., Giglio, L., van Leeuwen, T. T., Chen, Y., Rogers, B. M., et al. (2017). Global fire emissions estimates during 1997–2016. *Earth System Science Data*, 9(2), 697–720. <https://doi.org/10.5194/essd-9-697-2017>
- Wang, X., Heald, C. L., Liu, J., Weber, R. J., Campuzano-Jost, P., Jimenez, J. L., et al. (2018). Exploring the observational constraints on the simulation of brown carbon. *Atmospheric Chemistry and Physics*, 18(2), 635–653. <https://doi.org/10.5194/acp-18-635-2018>
- Wang, X., Heald, C. L., Ridley, D. A., Schwarz, J. P., Spackman, J. R., Perring, A. E., et al. (2014). Exploiting simultaneous observational constraints on mass and absorption to estimate the global direct radiative forcing of black carbon and brown carbon. *Atmospheric Chemistry and Physics*, 14(20), 10989–11010. <https://doi.org/10.5194/acp-14-10989-2014>
- Wang, X., Heald, C. L., Sedlacek, A. J., de Sá, S. S., Martin, S. T., Alexander, M. L., et al. (2016). Deriving brown carbon from multiwavelength absorption measurements: Method and application to AERONET and Aethalometer observations. *Atmospheric Chemistry and Physics*, 16(19), 12733–12752. <https://doi.org/10.5194/acp-16-12733-2016>
- Ward, D. S., Kloster, S., Mahowald, N. M., Rogers, B. M., Randerson, J. T., & Hess, P. G. (2012). The changing radiative forcing of fires: Global model estimates for past, present and future. *Atmospheric Chemistry and Physics*, 12(22), 10857–10886. <https://doi.org/10.5194/acp-12-10857-2012>
- Wiedinmyer, C., Yokelson, R. J., & Gullett, B. K. (2014). Global emissions of trace gases, particulate matter, and hazardous air pollutants from open burning of domestic waste. *Environmental Science & Technology*, 48(16), 9523–9530. <https://doi.org/10.1021/es502250z>
- Williamson, G. J., Bowman, D. M. J. S., Price, O. F., Henderson, S. B., & Johnston, F. H. (2016). A transdisciplinary approach to understanding the health effects of wildfire and prescribed fire smoke regimes. *Environmental Research Letters*, 11(12), 125009. <https://doi.org/10.1088/1748-9326/11/12/125009>
- Womack, C. C., Manfred, K. M., Wagner, N. L., Adler, G., Franchin, A., Lamb, K. D., et al. (2020). Complex refractive indices in the ultraviolet and visible spectralregion for highly absorbing non-spherical biomass burning aerosol [Preprint]. *Atmospheric Chemistry and Physics Discussions*. <https://doi.org/10.5194/acp-2020-1200>
- Wu, H., Taylor, J. W., Langridge, J. M., Yu, C., Allan, J. D., Szpek, K., et al. (2021). Rapid transformation of ambient absorbing aerosols from West African biomass burning. *Atmospheric Chemistry and Physics Discussions*, 1–37. <https://doi.org/10.5194/acp-2021-49>

- Wu, H., Taylor, J. W., Szpek, K., Langridge, J. M., Williams, P. I., Flynn, M., et al. (2020). Vertical variability of the properties of highly aged biomass burning aerosol transported over the southeast Atlantic during CLARIFY-2017. *Atmospheric Chemistry and Physics*, *20*(21), 12697–12719. <https://doi.org/10.5194/acp-20-12697-2020>
- Yuan, W., Huang, R.-J., Yang, L., Guo, J., Chen, Z., Duan, J., et al. (2020). Characterization of the light-absorbing properties, chromophore composition and sources of brown carbon aerosol in Xi'an, northwestern China. *Atmospheric Chemistry and Physics*, *20*(8), 5129–5144. <https://doi.org/10.5194/acp-20-5129-2020>
- Yue, X., Mickley, L. J., Logan, J. A., & Kaplan, J. O. (2013). Ensemble projections of wildfire activity and carbonaceous aerosol concentrations over the western United States in the mid-21st century. *Atmospheric Environment*, *77*, 767–780. <https://doi.org/10.1016/j.atmosenv.2013.06.003>
- Zuidema, P., Sedlacek, A. J., Flynn, C., Springston, S., Delgadillo, R., Zhang, J., et al. (2018). The Ascension Island boundary layer in the remote southeast Atlantic is often smoky. *Geophysical Research Letters*, *45*(9), 4456–4465. <https://doi.org/10.1002/2017GL076926>